Master's thesis

2023

Elias Lundheim

NTNU
Norwegian University of
Science and Technology
Faculty of Natural Sciences
Department of Physics

Elias Lundheim

Corner Load Sharing in the Fiber Bundle Model

June 2023

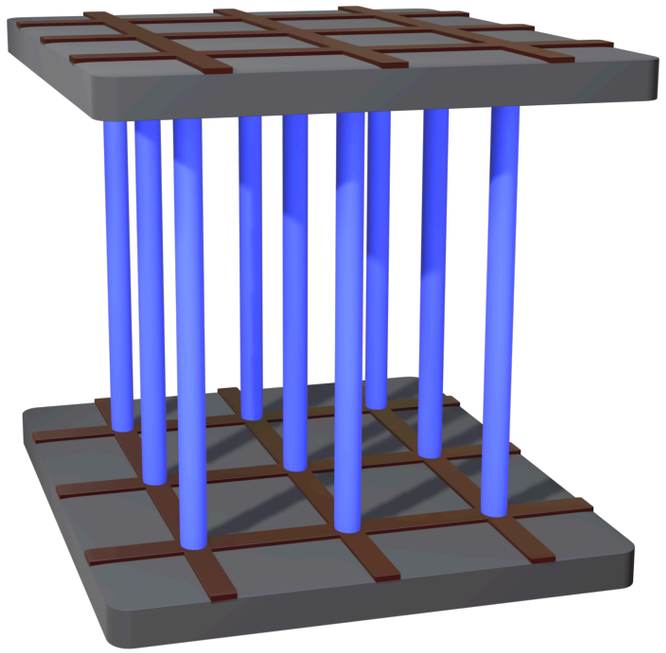

NTNU
Norwegian University of
Science and Technology

NTNU
Norwegian University of
Science and Technology

NTNU
Norwegian University of
Science and Technology

Corner Load Sharing in the Fiber Bundle Model

Elias Lundheim

Physics
Submission date: June 2023
Supervisor: Alex Hansen
Co-supervisor: Santanu Sinha

Norwegian University of Science and Technology
Department of Physics

Corner Load Sharing in the Fiber Bundle Model

Elias Lundheim
Supervisors: Santanu Sinha, Alex Hansen

22.06.2023

Preface

This Masters' thesis covers an introduction to the Fiber Bundle Model, and a computational and statistical exploration of a novel variation on the Fiber Bundle Model: Corner Load Sharing. It is expected that the reader has an undergraduate level of physics knowledge.

The thesis is the result of a years work at PoreLab – Centre of Excellence (SFF) at NTNU (2022-2023), where I have been surrounded by good friends, inspiring colleagues and mentors. I would like to thank everyone at PoreLab for interesting discussions at lunch, my fellow MSc students for board games and ping pong, my supervisors Santanu Sinha and Alex Hansen for excellent guidance, and Marie-Laure for baking cake every Monday. I would like to thank my parents and girlfriend Maiken for support under stressful and difficult days, but my friend Lars Schröder deserves a special thanks. He has spent hours reading my thesis together with me, and provided invaluable feedback. This thesis would have been a disaster without him.

Trondheim *Elias Lundheim*
June 22, 2023

Abstract

Understanding fracture mechanics can lead to stronger materials and safer buildings. Fracture mechanics is the reason why the windows on airplanes are rounded, and why the bags of taco spice have the tiny tear notches at the edges. The Fiber Bundle Model is a simple model that captures a fundamental effect of fracture mechanics. It will not be able to help you find the optimal shape of an airplane window, but it can help you understand *why* a rounded shape is better.

This thesis covers an introduction to the Fiber Bundle Model, Local Load Sharing and an exploration of a new model: Corner Load Sharing (CLS). Corner Load Sharing, as the name implies, emphasises that corners should experience more load than edges, but is otherwise identical to Local Load Sharing (LLS). Our main results are that 1: The dimensionality of CLS bundles varies continuously with disorder. 2: Localization in CLS very closely follows, or with a tuned definition of localization, precedes critical failure in a way LLS does not. And 3: That the critical strength of CLS bundles follow $\langle \sigma_c \rangle \propto 1/\ln(\ln(N))$. We leave several questions open for further research: Why does the dimensionality vary continuously? Why does $\langle \sigma_c \rangle$ not scale with N in LLS when it does in CLS? And why does the brittle region seem to stop exacly at $t_0 = \langle \sigma_i^{\text{th}} \rangle / 2$?

Contents

1 Introduction

When one asks what is at the forefront of physics, what is yet unexplained and unexplored, one might often hear answers involving quantum physics, superconductivity, particle physics, fusion or dark matter. Fortunately, spaghettifying black holes and star-like fusion reactors are things one commonly never interact with in every day life, but because of this association with what is at the cutting edge of physics, one might be lead to a misconception: that the physics of comparatively mundane phenomena are well understood. This is not the case. The physics of flowing sand in an hourglass, water percolating through a sponge, and the topic of this thesis, how things break, are all areas of active research today [1–3]. How things break, or formally *fracture mechanics*, is a wide field of study. When you, dear reader, walk over a bridge, fracture mechanics is what determines whether or not the bridge collapses. If your phone falls out of your hand, fracture mechanics is what determines if the phone screen breaks or survives. Earthquakes can be thought of as the result of elastic shear instabilities, a strain on the earths crust that eventually breaks the crust in a violent manner, resulting in an earthquake. There are still many aspects of fracture in materials which are not well understood. One of the key challenges in modeling fracture is the wide range of scales at which they occur. Fracture begins with individual molecules being torn apart, to cell walls or crystals breaking, all the way to a snapping chain or even an earthquake. When modeling a macroscopic fracture event, it is, for the foreseeable future, impossible to model every atom. Instead, we must use models that mimic the emergent behaviour that we observe and care about.

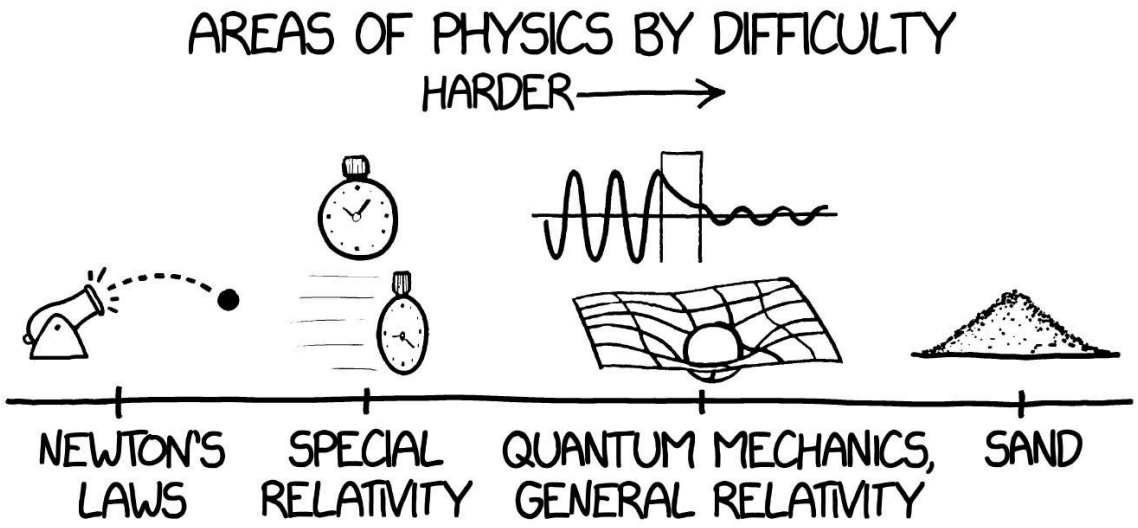

Figure 1.1: Comic by Randall Munroe from The New York Times.

There are many ways to explore fracture mechanics and failure in materials. A macroscopic top down approach such as using Linear Elastic Fracture Mechanics (LEFM) [4, 5] or a microscopic bottom up approach using atomistic modeling [6, 7] are both viable approaches that see use today. The Fiber Bundle Model (FBM) [3] is a model in between these two extreme approaches. It first originated as a model used for textiles in the mid 1920s [8] and consists of a bundle of fibers that act as ideal springs. If the fibers are identical, they will all fail at the same time, but if we add some randomness to the breaking points of the fibers, the bundle exhibits interesting emergent behaviours that gives insight into a surprisingly wide area of fracture mechanics. After it's introduction it saw further analytical analysis in 1945 [9] and quickly gained more attention as computers became more accessible and capable during the late 1980s [10, 11]. Despite being simple, the FBM provides deep and general insights into fracture and failure in a variety of systems. If we replace the springs with electrical wires, spring constant with resistance, mechanical stress with current and strain with electric voltage, the FBM becomes a Random Fuse Model, a model that also sees new research [12]. If the fibers are replaced by roads, it can be used to model traffic jams [13]. If the fibers are replaced by power lines, it can be used to model electrical grids [14]. The FBM is not only relevant for textiles, but captures some general behavior of cascading failure that we see in a wide range of systems, including materials. The price to pay for its generality is the limited accuracy, but accuracy is of little concern if the goal is to understand the rules of failure.

One of the key features of the FBM is its ability to mimic disorder in a material. We mentioned that each fiber in the FBM breaks individually. To build further on this, we say that each fiber receives an individual strength, drawn from a chosen distribution. If we give all the fibers the same strength, i.e. use a distribution with low variance, the fibers will break all at once, and we can study brittleness. If we have a distribution with high variance, we can study fracture of ductile materials. Because we can smoothly increase or decrease the variance in the distribution, we can observe how the strength of a bundle behaves as a function of the disorder in the material. Keep in mind however, that to directly compare a bundle to any real material is often very optimistic and fruitless. In some sense, most FBMs are perfectly elastic and plastic at the same time, something quite unheard-of in real materials. Elastic because it will always contract back to its original shape, and plastic because once a fiber breaks, it is not restored or healed. This is the case for most implementations of the FMB, but there are exceptions: one variation on the FBM introduces continuous damage instead of a single breaking threshold [15], another introduces a healing mechanism to model snow [16], but making the FBM more complex and realistic is not without drawbacks. The real value of the FBM

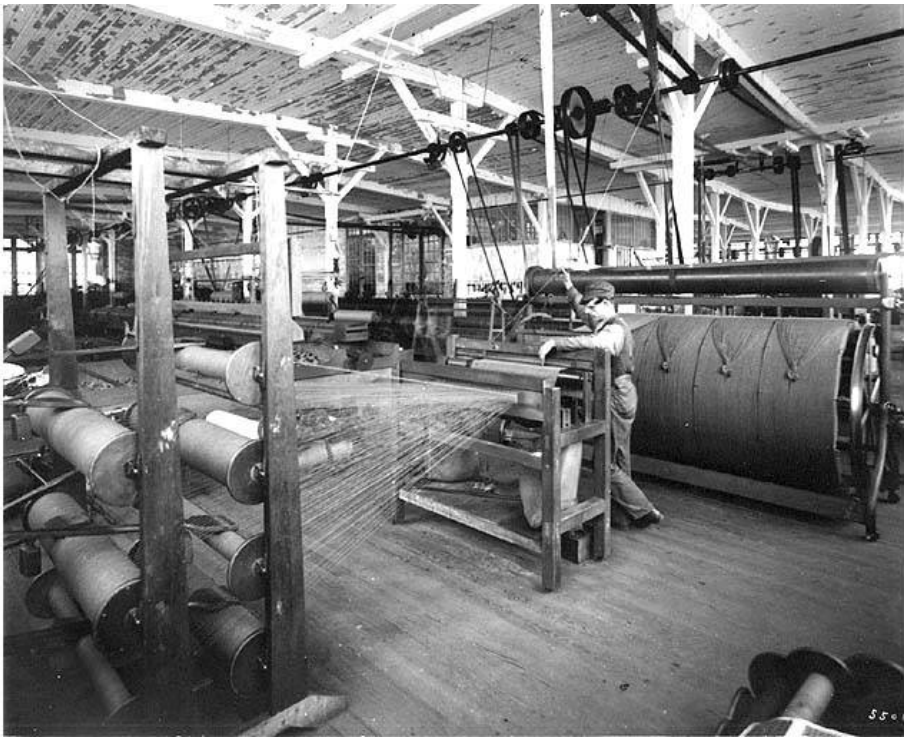

Figure 1.2: A 1900s warp dresser weaving wool into something similar to what a FBM was initially intended to model. *Photographer: Asahel Curtis.*

comes from its simplicity. Other models may be more accurate, but are also more difficult to understand and analyse. Any model should strive to be as simple as possible, and added complexity must be weighed against its improved performance.

This thesis will explore a variation of the FBM and suggest whether or not the features introduced in the variation justify the added complexity. The feature we want to explore is stress concentration on corners. It is generally accepted that corners are a common failure point in many designs because they create stress concentrations. To mimic this, we introduce a FBM that distributes more load onto fibers that have fewer adjacent fibers, and less load onto fibers surrounded by other fibers. We first give a introduction to the fiber bundle models that we will be exploring, while also introducing some useful terms and concepts related to FBMs. We introduce and provide an overview of the code used to simulate bundle breaking, and finally present the data and results obtained from the simulations, along with a comprehensive discussion and interpretation of the findings.

2 The Fiber Bundle Model

The fiber bundle model (FBM) consists of springs that are attached between two surfaces. The surfaces are pulled apart such that the springs start to stretch. This thesis will focus its attention on N ideal springs arranged in a $L \times L$ square 2D lattice, as shown in figure 2.1.

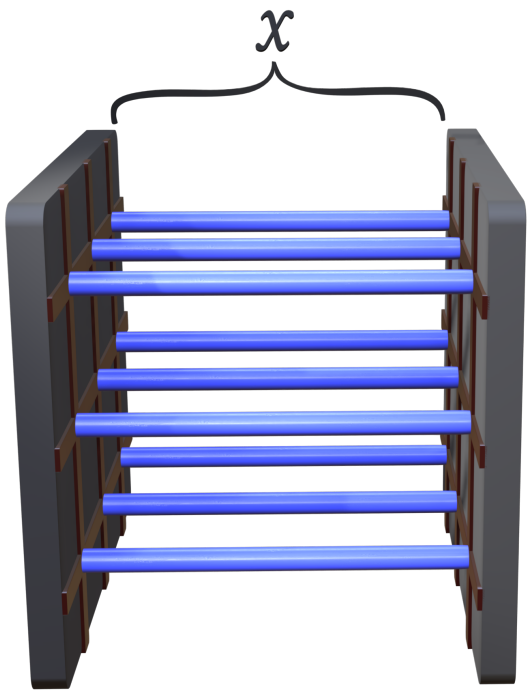

Figure 2.1: A figure of nine blue fibers stretched between two parallel plates. The plates are separated by a distance x.

Each fiber i pulls back on the plates with a force σ_i following Hooke's law:

$$\sigma_i = \kappa x_i, \tag{1}$$

where κ is a spring constant and x_i is the distance fiber i has been stretched. For now, all fibers stretch by the same distance x. The bundle contracts against an external force F, such that the average load on the fibers σ is

$$\sigma \equiv \frac{F}{N} = \sum_{i=1}^{N} \frac{\sigma_i}{N}. \tag{2}$$

There is little room for complexity if the fibers are just ideal springs, so the next step is to let the fibers break once the load they carry σ_i reaches a certain threshold value σ_i^{th}. We draw these threshold values from a distribution P and for now, we let P simply be the uniform distribution on the interval $[0, 1]$. When the fibers break, their load is set to zero for the remainder of the breaking process. If we let k be the

number of broken fibers, we can obtain a new expression for the average load of the fibers

$$\sigma = \frac{\kappa x(N-k)}{N}, \tag{3}$$

where N is the number of fibers. We see $N-k$ as the number of intact fibers and κx acting as the force from a fiber. If we plot the average load on the fibers as we increase x, we obtain the plot in figure 2.2. Each time a fiber breaks, there is a discontinuous drop in σ, and as k increases, the slope in between each drop decreases, as indicated by dashed guiding lines.

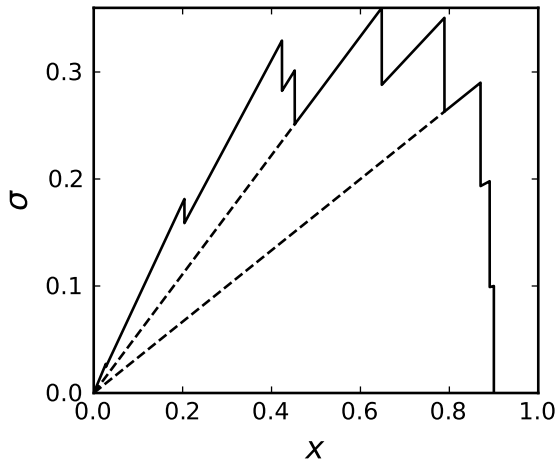

Figure 2.2: Average load from $N = 9$ fibers. The dashed lines indicate the slope of the line segments between vertical drops in σ.

2.1 Control Variables

We need to address which variables we control, and how we control them. See figure 2.3 for an illustration of what a force controlled and displacement controlled experiment could look like. The fibers are attached between two clamps. In the force controlled experiment, the weight represents an external pulling force F that pulls the clamps apart. In the displacement controlled experiment, the clamps are attached to a vice where only the right clamp moves.

The simulation shown in figure 2.2 uses a displacement controlled experiment, since when a fiber breaks, σ drops and x is constant. A displacement controlled experiment is a good way of visualizing what happens in a breaking bundle, but most real world situations are force controlled. A force controlled experiment uses a steadily increasing external pulling force F, and measures at what elongation x the equilibrium $\sum_i^N \sigma_i = F$ is reached. As we saw in figure 2.2, the bundle reaches its

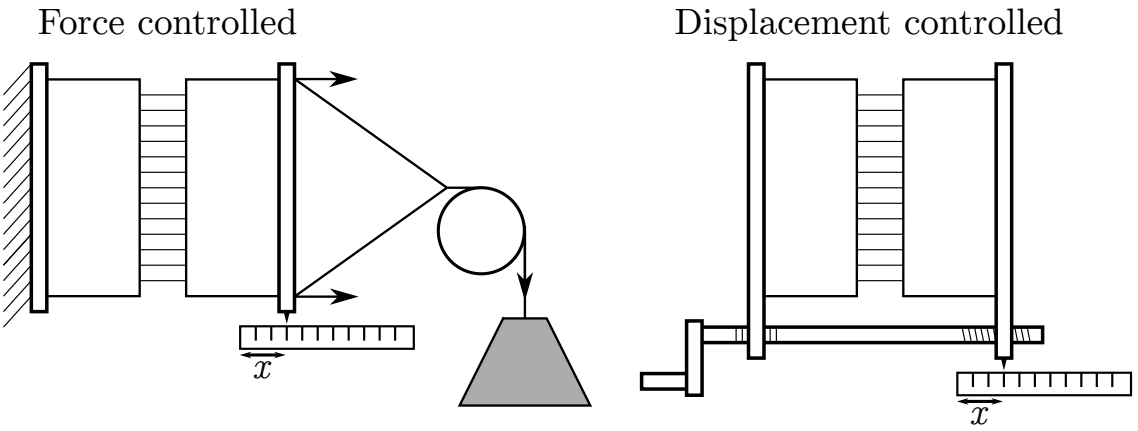

Figure 2.3: Two ways to set up a simple experiment. Fibers are attached to clamps that are pulled apart with a vice or a weight representing an external force F. The elongation of the fibers x can be measured with a ruler as shown.

maximum load around $x = 0.62$. We call this the critical load of the bundle σ_c, see section 2.7.1. Once $\sigma > \sigma_c$, the bundle will never achieve equilibrium, and all the fibers will immediately break. This is illustrated in figure 2.4 where we break the same bundle as in figure 2.2, but using a force controlled experiment. When $\sigma \geq \sigma_c = 0.35$, the rest of the fibers break, and x goes to infinity.

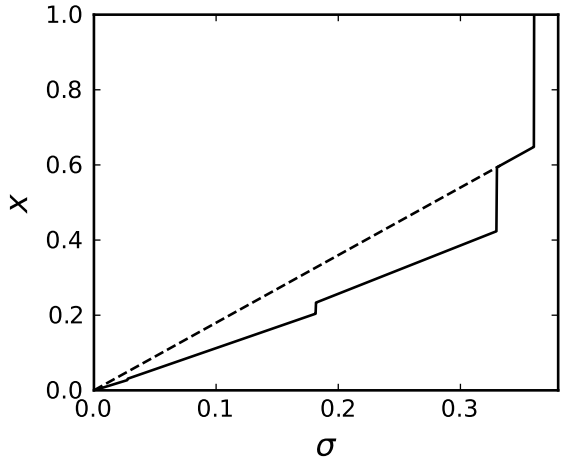

Figure 2.4: The same bundle as in figure 2.2, but broken using a force controlled experiment. The dashed line illustrates that the slope of the line segment between the last two jumps is steeper than previous line segments.

Since we use simulations, we can avoid using either force or displacement control. In our simulation we find the σ required to break the next fiber without having to slowly increase x or σ, see section 2.6. This lets us plot σ over k, as shown in figure 2.5. This will be the way we present all future bundle breaks, using k in the x-axis, often rescaled to $\frac{k}{N}$.

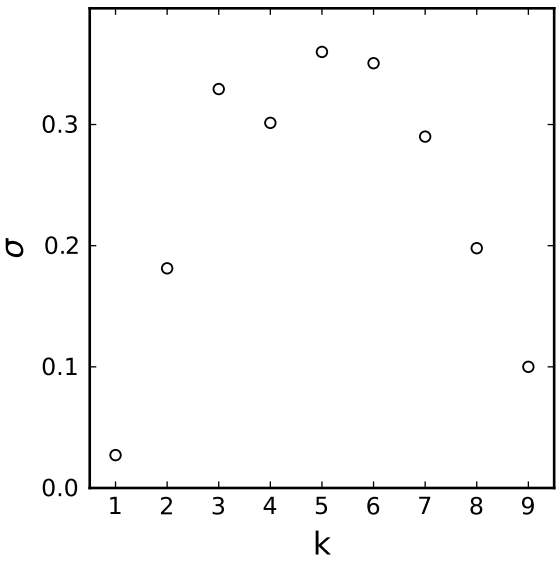

Figure 2.5: The same bundle as in figure 2.2, showing the force required to break each of the $N = 9$ fibers.

2.2 Equal Load Sharing

In the previous section, we presented an expression for σ, see eq. (3), where the force from a single fiber was κx. This is true so long as all fibers are equally stretched, in which case we would call the situation Equal Load Sharing (ELS). As we will see, this will not always be the case, so in preparation for un-equal loading, we need an expression for the load on an individual fiber. Of course, $\sigma_i = \kappa x_i$ where x_i is the elongation of fiber i would be valid, but we would prefer an expression for σ_i as a function of σ. We can use equation (3) as our starting point, replace κx with σ_i, and solve for σ_i:

$$\sigma = \frac{\sigma_i(N-k)}{N} \tag{4}$$

$$\sigma_i = \sigma(1 + \frac{k}{N-k}) \tag{5}$$

We have now obtained our expression for the load on individual fibers using ELS:

$$\sigma_i = \begin{cases} \sigma(1 + \frac{k}{N-k}), & \text{intact} \\ 0, & \text{broken} \end{cases} \tag{6}$$

where k is the number of broken fibers in the bundle. As an example, consider the very last fiber, such that $k = N - 1$. The load on the last fiber is

$$\sigma_i = \sigma(1 + \frac{N-1}{N-N+1}) = \sigma N, \tag{7}$$

in other words, the total force F. A helpful way to see equation (6) is to note that we have the average force on the fibers σ in the first term, plus some additional term dependant on how many fibers have broken. In the types of load sharing we present in this thesis, σ_i will always have a contribution from the fiber itself, plus some additional load from broken fibers.

2.3 Local Load Sharing

In an ELS bundle with one broken fiber, all fibers, regardless of how far away from the broken fiber they are, will receive the same amount of extra load. Intuitively, one would expect fibers closer to the broken fiber to receive more load than the fibers further away. ELS is only realistic[1] if the clamps are very stiff, not allowing some fibers to stretch more than others. This is illustrated in figure 2.6. Consider what would happen if one of the clamps were soft. We would then end up in the situation depicted in figure 2.7. When we use a soft clamp, we observe an interesting effect. Fibers that are adjacent to broken fibers experience more load than fibers that are adjacent to intact fibers. This type of *soft clamp model* has been explored by Batrouni et al. in 2002 [17] and Patinet et al. in 2014 [18] and has been used to successfully replicate experimental data [19]. And while it has the desired behaviour of putting additional stress on isolated fibers, it quite analytically complex, computationally expensive and difficult to implement. A simpler way to obtain a similar effect, is to only give extra load to fibers directly adjacent to broken fibers. Doing so will create a clamp that looks something like the illustration in figure 2.8. When a fiber breaks, we distribute the load of the broken fiber to the adjacent neighbours of the broken fiber, instead of distributing it equally among all the fibers.

2.3.1 History Dependency in the LLS Implementation

The exact way in which LLS is implemented is not widely agreed upon. Our implementation is history-independent but many other LLS implementations are not. This issue is discussed more thoroughly by Hansen [3], but we also explain the issue here. Let us look at a quick example using two 1D bundles with only six fibers, see table 2.1. Each row shows the load of all the fibers in a bundle, and moving down one row increases the number of broken fibers k by one. In the history dependent version, we split the load that the breaking fiber carried equally onto its nearest

[1]The FBM is a simple model that is useful for understanding fundamental fracture mechanics. It does not model natural materials. When saying that an aspect of the FBM is more or less "realistic", it should be regarded in the context of a FBM, not compared to, for example, atomistic modeling.

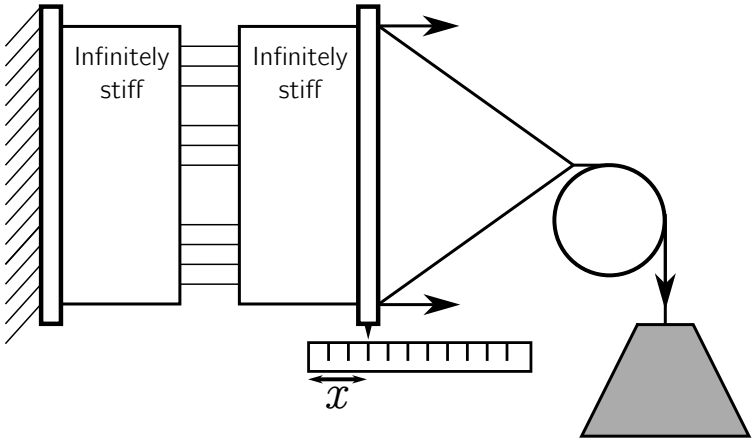

Figure 2.6: Fibers attached to infinitely stiff clamps clamps that are pulled apart with an external force F. The value of x is measured by the displacement of the right clamp.

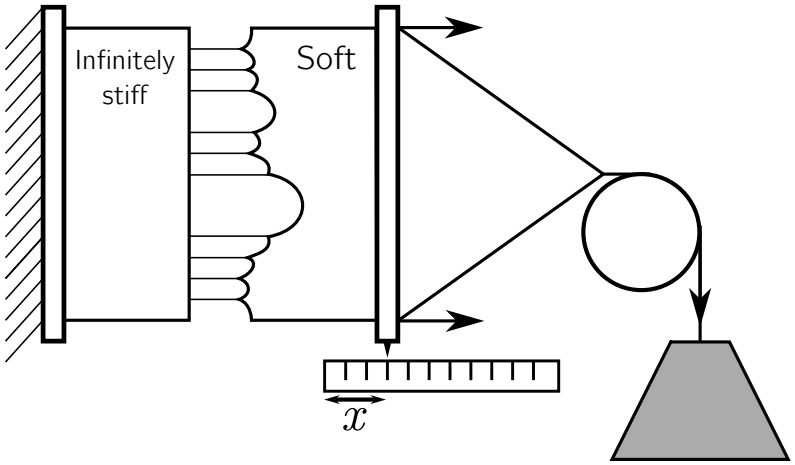

Figure 2.7: The same device as in figure 2.6, but with a soft right clamp.

neighbours. In the history independent version of LLS, we imagine that a breaking fiber expands or creates a hole. This hole can be interpreted as a crack, but the formal nomenclature is to call the hole a *cluster* of broken fibers. We then calculate the total load that the broken fibers in the cluster would have carried if they were not broken, and split that load onto the neighbours of the cluster.

The problem with a history dependent implementation, shown to the left in table 2.1, is that unless you knew the order in which the fibers were broken, you could not know which fiber carried a load of 7/4, and which carried a load of 9/4. By first finding the total load from the broken fibers in a cluster, and then distributing the load onto the neighboring fibers, we avoid creating situations where one would need to know the order of the breaking process.

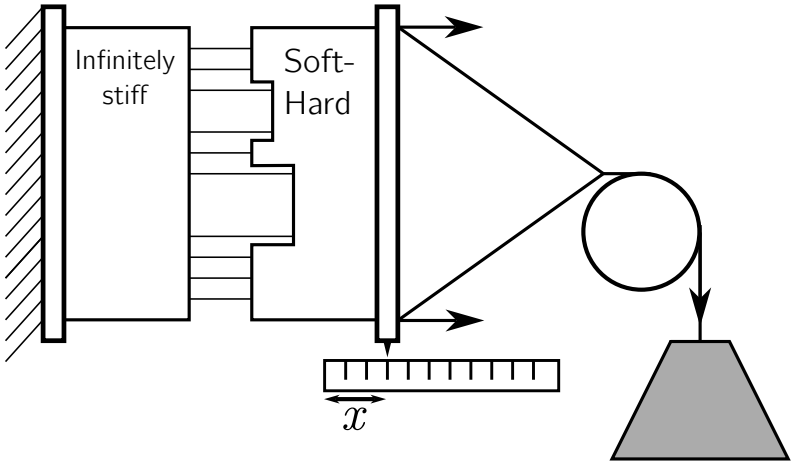

Figure 2.8: The same device as in figure 2.6, but with a soft-hard right clamp.

k	History dependent						History independent					
0	1	1	1	1	1	1	1	1	1	1	1	1
1	1	1	$\frac{3}{2}$		$\frac{3}{2}$	1	1	1	$\frac{3}{2}$		$\frac{3}{2}$	1
2	1	$\frac{7}{4}$			$\frac{9}{4}$	1	1	2			2	1

Table 2.1: Two 1D bundles using a history dependent and independent version of LLS. Each row shows the load on all the fibers in the bundle, and moving down one row shows the sate of the bundle after another fiber has broken.

2.3.2 Two Dimensional Clusters and Perimeters

This thesis considers 2D FBMs, and as such, we must define a cluster in two dimensions, and introduce the cluster's *perimeter*. The definition of a two dimensional cluster is more easily understood with a figure, for while it is quite simple when you see it, it is a bit tricky to explain with words. Let the grid in figure 2.9 represent a bundle. Blank cells will be intact fibers and labeled cells will represent broken fibers. Fibers labeled A will belong to cluster A, those labeled B belong to cluster B and so on. With this figure in mind: A cluster is a group of broken fibers that are connected by the 4 nearest neighbours in the lattice. Note also that FBMs use periodic boundary conditions, resulting in fibers (1,1) and (4,1) belonging to the same cluster C. The perimeter of a cluster consists of all fibers that are nearest neighbour to at least one fiber in the cluster. By definition, a fiber in one cluster cannot be on the perimeter of a different cluster. If that were the case, the two clusters would merge into one cluster. As an exercise to the reader, see if you can find the cell that is on the perimeter of all the clusters in the figure.

The idea of LLS is that the load from a cluster should be redistributed equally among all fibers in the perimeter of that cluster. We will construct a quick illustrat-

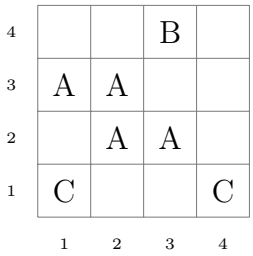

Figure 2.9: A bundle illustrating the concept of clusters.

ing example. To get nicer numbers, we introduce a relative load

$$\hat{\sigma}_i = \frac{\sigma_i}{\sigma}. \tag{8}$$

Equation (2) then gives us that $\sum_i^N \hat{\sigma}_i = N$. We have represented the bundle as a grid of these $\hat{\sigma}_i$ values for $k = 1$ and $k = 2$ in figure 2.10. The figure illustrates the difference between how stress is distributed using ELS and LLS. The reader should convince themselves that the sum of the values in the grids add up to N.

ELS $k = 1$

$\frac{16}{15}$	$\frac{16}{15}$	$\frac{16}{15}$	$\frac{16}{15}$
$\frac{16}{15}$	0	$\frac{16}{15}$	$\frac{16}{15}$
$\frac{16}{15}$	$\frac{16}{15}$	$\frac{16}{15}$	$\frac{16}{15}$
$\frac{16}{15}$	$\frac{16}{15}$	$\frac{16}{15}$	$\frac{16}{15}$

ELS $k = 2$

$\frac{16}{14}$	$\frac{16}{14}$	$\frac{16}{14}$	$\frac{16}{14}$
$\frac{16}{14}$	0	0	$\frac{16}{14}$
$\frac{16}{14}$	$\frac{16}{14}$	$\frac{16}{14}$	$\frac{16}{14}$
$\frac{16}{14}$	$\frac{16}{14}$	$\frac{16}{14}$	$\frac{16}{14}$

LLS $k = 1$

1	$\frac{5}{4}$	1	1
$\frac{5}{4}$	0	$\frac{5}{4}$	1
1	$\frac{5}{4}$	1	1
1	1	1	1

LLS $k = 2$

1	$\frac{8}{6}$	$\frac{8}{6}$	1
$\frac{8}{6}$	0	0	$\frac{8}{6}$
1	$\frac{8}{6}$	$\frac{8}{6}$	1
1	1	1	1

Figure 2.10: Four bundles using the ELS and LLS models. The numbers in each grid represents the relative load $\hat{\sigma}_i$ on the fibers.

2.3.3 Defining σ_i for LLS

A cluster $\mathcal{J}$ will have a size $s_\mathcal{J}$ and a perimeter length $h_\mathcal{J}$. Using figure 2.10 as an example, when $k = 1$ then $s_\mathcal{J} = 1, h_\mathcal{J} = 4$ and when $k = 2$ then $s_\mathcal{J} = 2, h_\mathcal{J} = 6$. If we distribute the load of the cluster equally on the fibers on the perimeter, then

$$\hat{\sigma}_j = 1 + \frac{s_\mathcal{J}}{h_\mathcal{J}}, \tag{9}$$

where j is a fiber on the perimeter of cluster $\mathcal{J}$. The last thing we need to introduce before we can describe LLS is some way to handle fibers that are adjacent to two or more clusters at the same time. See for example the fiber in cell (3,1) in figure 2.9 which is adjacent to three clusters. We introduce C_i as the set of clusters that are adjacent to fiber i, and with that define σ_i for LLS as

$$\sigma_i = \sigma(1 + \sum_{\mathcal{J} \in C_i} \frac{s_{\mathcal{J}}}{h_{\mathcal{J}}}). \tag{10}$$

We will no longer explicitly state that $\sigma_i = 0$ when fiber i is broken as in equation (6), but keep in mind moving forward that this will always be the case.

2.3.4 Local Load Sharing Example

As an illustrative example to show the effect of LLS, consider a one dimensional LLS bundle as shown in figure 2.11. The figure shows the same bundle in three situations, situation A where $k = 0$ and situations B and C where $k = 1$, using LLS and ELS respectively. The threshold value of each fiber is indicated by a dashed line and we can see that fiber 2 is the weakest fiber. When F reaches $F = 0.8$ such that $\sigma_2 = \sigma_2^{\text{th}} = 0.2$, fiber 2 breaks. In bundle B, due to local load sharing, the adjacent fibers 1 and 3 receive extra load. Therefore, even though σ is only 0.2, σ_1 and σ_3 are 0.3 because they need to pick up the slack that was created when fiber 2 broke in order to conserve the total load on the bundle. Check for yourself that $\sum_i^N \sigma_i = F$ holds in both situation A, where $F = 0.4$ and B, where $F = 0.8$. If we imagine pulling the bottom clamp in situation B further down, we see that because of the "bend" in the clamp, fiber 3 will end up breaking before fiber 4 even though fiber 4 is weaker than fiber 3. In bundle C using ELS, the clamp has been stretched to a value of $x = 0.2 + 0.2/3$.

2.3.5 Morphology of ELS and LLS

It can be useful to visualize what the bundles look like in order to understand how they function and differ. Progressive fracture of a ELS and a LLS bundle is shown in figure 2.12. ELS and LLS both start of very similar, but at $k/N = 0.4$ we see drastic differences. The ELS bundle is at this point characterised by many clusters, all of roughly the same size. On the other hand, the LLS bundle is dominated by a single very large cluster. This is because once a cluster reaches a certain size, the additional load on the perimeter of that cluster will cause all future fiber failures to occur on the that perimeter. This is referred to as *localization*, see section 2.7.4. It might seem as though localization also has occurred in the ELS bundle when $k/N = 0.6$, but this massive cluster has appeared not due to any specific cluster growing, but

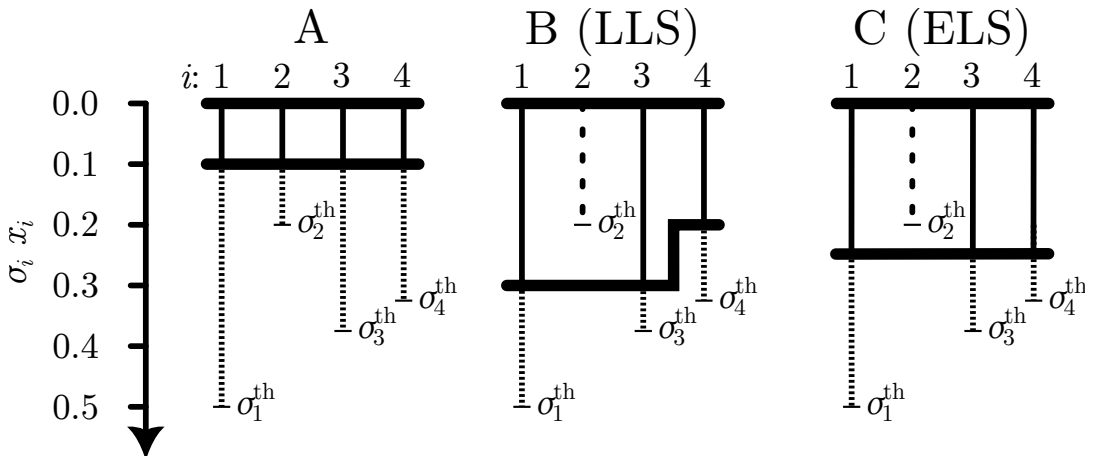

Figure 2.11: An illustration of two local load sharing bundles and a vertical axis showing the values of σ_i and x_i for intact fibers. Broken fibers have $\sigma_i = x_i = 0$. Bundle A has four intact fibers and holds a load $F = 0.4$. Dashed lines indicate the threshold values of the fibers. Bundles B and C are identical to bundle A, but $F = 0.8$ and fiber 2 has broken.

rather due to clusters randomly merging. When $k/N = 0.8$ and beyond, practically all the remaining fibers are part of the same perimeter, in which case ELS and LLS behave identical.

2.4 Threshold Distribution and Disorder

One of the most important parameters commonly used in FBM studies is the disorder of the bundle. The disorder of the bundle refers to whether or not the threshold distribution used has a large or a small variance. In this context, a uniform distribution between 0.49 and 0.51 has a small variance, and a uniform distribution between 0 and 1 has a large variance. Note that the mean of the distribution is 0.5 in both cases. If we attempt to answer whether homogeneous or inhomogeneous materials are stronger, it is critical that changing the disorder does not change the average strength of the fibers. Any strength related effect the disorder might have would be hidden and distorted by the other changes that we unintentionally made at the same time. In this thesis we will for simplicity mainly be using a uniform distribution centered around 0.5 with a radius of $0 \leq t_0 \leq 0.5$:

$$p(x) = \begin{cases} \frac{1}{2t_0}, & 0.5 - t_0 < x < 0.5 + t_0 \\ 0, & \text{otherwise} \end{cases} \tag{11}$$

But there are many other distributions commonly used in FBMs such as exponential, inverse, power-law and Weibull distributions.

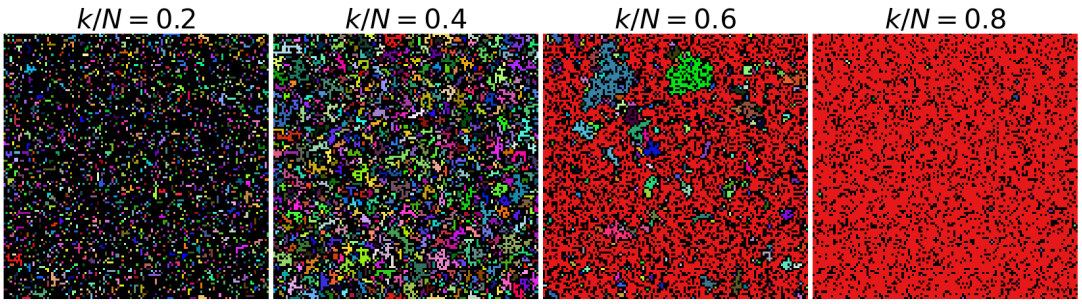

(a) ELS

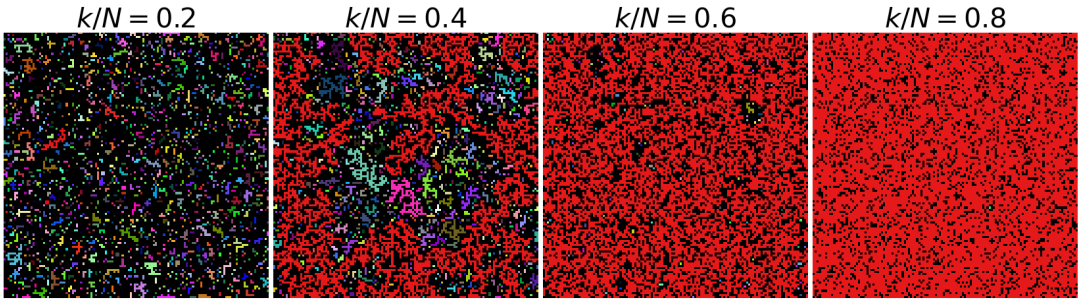

(b) LLS

Figure 2.12: Progression of breaking for ELS and LLS, $N = 128^2$. Black pixels are intact fibers and pixels of the same color belong to the same cluster. The largest cluster is always colored red.

Changing the distribution of a bundle can have drastic effects on the morphology of clusters. This is illustrated in figure 2.13 where we see bundles that have been generated using the same seed, but scaled into differing uniform distributions dictated by the t_0 parameter. Note that disorder has no effect in ELS bundles, and they are therefore not plotted.

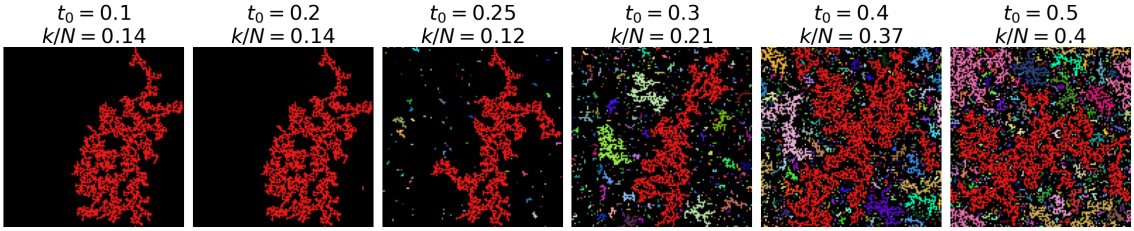

Figure 2.13: Six LLS bundles generated using the same random seed, but where the thresholds are scaled to various degrees of disorder t_0.

2.5 Corner Load Sharing

The motivation for Corner Load Sharing (CLS) is quite similar to the one used for LLS, see the introduction to section 2.3. When the attachment point of the fibers is soft, fibers adjacent to broken fibers receive more load than fibers adjacent to intact fibers. LLS does this very well in a one dimensional bundle, but in a two dimensional bundle, LLS does not distinguish between fibers that are completely isolated, i.e. surrounded by broken fibers on all sides and diagonals, and a fiber that only has one broken neighbour, and 8 intact ones, see figure 2.14. If we want to follow the motivation originally used for LLS, we should distinguish these situations. This thesis explores a way to do this suggested by Kjellstadli [20]. We simply take load off fibers with more neighbours, and give it to fibers with fewer neighbours.

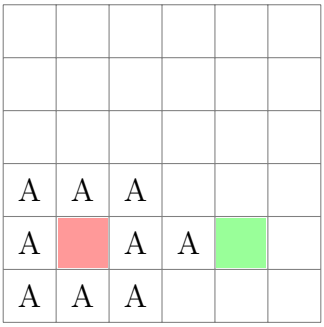

Figure 2.14: A $N = 36$ bundle with a cluster of broken fibers labeled A. The red fiber is surrounded by broken fibers on all sides, including diagonals, where as the green fiber is almost completely surrounded by intact fibers. In LLS, the red and green fibers experience the same amount of load.

Local Load Sharing has a *uniform* distribution of load onto the perimeter of clusters. We will create a new distribution that is not uniform, but instead focuses load onto fibers with fewer neighbours. This includes both isolated fibers, and fibers at the corners of clusters. Therefore, we will call the model Corner Load Sharing (CLS). CLS uses a new distribution $g_{i\mathcal{J}}$ that is dependent on the number of fibers in the neighbourhood of each fiber in the perimeter. In this implementation we will be considering the four closest neighbours and the four diagonally adjacent neighbours (next nearest neighbours) when counting the number of intact fibers n_i surrounding a fiber i, but also including itself, such that $1 \leq n_i \leq 9$. The distribution function $g_{i\mathcal{J}}$ (as suggested by Kjellstadli [20]) has the form

$$g_{i\mathcal{J}} = n_i^{-\alpha} c_{\mathcal{J}}, \tag{12}$$

where $c_{\mathcal{J}}$ is a normalization constant and $\alpha \geq 0$ is a tunable parameter. It follows that if the number of neighbours n_i is large, $g_{i\mathcal{J}}$ will be small and vice versa. The

normalization constant $c_{\mathcal{J}}$ is determined for each cluster $\mathcal{J}$ and is defined as

$$c_{\mathcal{J}} = \frac{1}{\sum_{j \in P_{\mathcal{J}}} n_j^{-\alpha}}, \tag{13}$$

where $P_{\mathcal{J}}$ is the set of all fibers on the perimeter of cluster $\mathcal{J}$. The complete expression for σ_i using CLS is

$$\sigma_i = \sigma(1 + \sum_{\mathcal{J} \in C_i} s_{\mathcal{J}} g_{i\mathcal{J}}), \tag{14}$$

where $s_{\mathcal{J}}$ is the size of cluster $\mathcal{J}$ and C_i is the set of clusters directly adjacent to fiber i. Note that CLS contains LLS, since if $\alpha = 0$, then

$$c_{\mathcal{J}} = \frac{1}{\sum_{j \in P_{\mathcal{J}}} n_j^0} = \frac{1}{h_{\mathcal{J}}} \implies g_{i\mathcal{J}} = n_i^0 c_{\mathcal{J}} = \frac{1}{h_{\mathcal{J}}} \tag{15}$$

$$\sigma_i = \sigma(1 + \sum_{\mathcal{J} \in C_i} s_{\mathcal{J}} g_{i\mathcal{J}}) = \sigma(1 + \sum_{\mathcal{J} \in C_i} \frac{s_{\mathcal{J}}}{h_{\mathcal{J}}}). \tag{16}$$

We recognise this from equation (10) as LLS. As $\alpha \to \infty$, the distribution becomes more extreme, such that *all* the load is given to the fibers with the fewest number of neighbours.

2.5.1 Load Conservation

It is important that the total load from a cluster does not change and that the load is only shifted, not added or removed. We will go though a quick example in both LLS and CLS to show that despite their differences, they both agree on the total load from a single cluster. For simplicity we again use relative loads $\hat{\sigma}_i$. If we sum up the total load $\hat{\sigma}_{\mathcal{J}}$ from the fibers around a LLS cluster $\mathcal{J}$ we end up with

$$\text{LLS}: \quad \hat{\sigma}_{\mathcal{J}} = \sum_{j \in P_{\mathcal{J}}} \hat{\sigma}_j = \sum_{j \in P_{\mathcal{J}}} (1 + \sum_{\mathcal{J} \in C_j} \frac{s_{\mathcal{J}}}{h_{\mathcal{J}}}) = h_{\mathcal{J}} + s_{\mathcal{J}} \tag{17}$$

using that $\sum_{j \in P_{\mathcal{J}}} 1 = h_{\mathcal{J}}$ and that $C_j = \{\mathcal{J}\}$ since we only consider the sum of the force from a single cluster. The reader may use figure 2.10 to verify this result for themselves. We now do the same for CLS:

$$\text{CLS}: \quad \hat{\sigma}_{\mathcal{J}} = \sum_{j \in P_{\mathcal{J}}} \hat{\sigma}_j = \sum_{j \in P_{\mathcal{J}}} (1 + \sum_{\mathcal{J} \in C_j} s_{\mathcal{J}} g_{j\mathcal{J}}) = h_{\mathcal{J}} + \sum_{j \in P_{\mathcal{J}}} s_{\mathcal{J}} g_{j\mathcal{J}}, \tag{18}$$

again using the same arguments as for LLS. Continuing,

$$
\begin{aligned}
h_{\mathcal{J}} + \sum_{j \in P_{\mathcal{J}}} s_{\mathcal{J}} g_{j\mathcal{J}} &= h_{\mathcal{J}} + s_{\mathcal{J}} \sum_{j \in P_{\mathcal{J}}} n_j^{-\alpha} c_{\mathcal{J}} \\
&= h_{\mathcal{J}} + s_{\mathcal{J}} \frac{\sum_{j \in P_{\mathcal{J}}} n_j^{-\alpha}}{\sum_{j \in P_{\mathcal{J}}} n_j^{-\alpha}} = h_{\mathcal{J}} + s_{\mathcal{J}}
\end{aligned}
\tag{19}
$$

which is the same expression that we found for LLS.

2.5.2 Example of Load Distribution in CLS

As a final introductory example of the CLS behaviour, consider the bundles shown in figure 2.15. Note that we use periodic boundary conditions and that $\alpha = 1$. As expected, the fiber in the CLS bundle with the fewest number of neighbours takes more load than the other fibers.

LLS

1	$\frac{10}{7}$	$\frac{10}{7}$	1
$\frac{10}{7}$	0	0	$\frac{10}{7}$
1	$\frac{10}{7}$	0	$\frac{10}{7}$
1	1	$\frac{10}{7}$	1

CLS

1	1.4	1.4	1
1.3	0	0	1.4
1	1.5	0	1.4
1	1	1.3	1

Figure 2.15: Two bundles using LLS and CLS. The numbers in each grid represents the relative load $\hat{\sigma}_i$ on the fibers. The red fiber takes on the most amount of load, and the green fibers take on the least amount of load. The values in the CLS bundle have been rounded down from 1.380, 1.434 and 1.506 for presentation. For reference $10/7 = 1.429$.

2.5.3 Preview of CLS

For the eager reader, curious to see what CLS clusters look like, we present a small preview of our results. Figure 2.16 shows the breaking progress of a LLS and a CLS bundle. CLS and LLS are in a sense quite similar, one might at least expect larger differences between LLS and ELS, as they are considered to be two opposing extremes. After all, the only difference between CLS and LLS is that LLS uses a uniform distribution of load on the perimeters of clusters, while CLS uses a distribution that concentrates load onto isolated fibers. Despite this, the visual difference in the shape of the clusters in figure 2.16 considerably more distinct than the difference between the clusters of LLS and ELS, see figure 2.12.

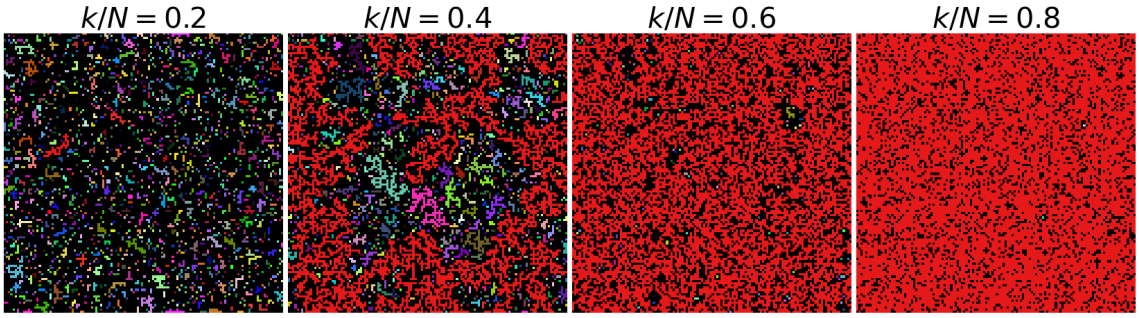

(a) LLS

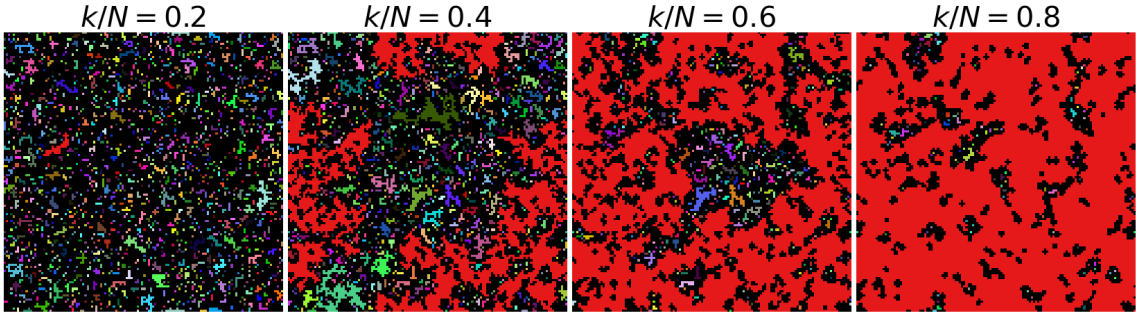

(b) CLS

Figure 2.16: Progression of breaking for LLS and CLS. k is the number of broken fibers. $N = 128^2$ is the total number of fibers in the system. Black pixels are intact fibers and pixels of the same color belong to the same cluster. The largest cluster is always colored red.

2.6 The Order of Breaking

In a naive approach to simulating a FBM, one might slowly increase the value of σ until a fiber breaks. However, with some calculations, we can find what fiber should break first and at what value of σ it should break. In between points of breaking, the bundle acts as a simple ideal spring with spring constant $K = \kappa(N - k)$, so the real challenge of modeling the FBM is finding when, and in which order the fibers break. With that in mind, observe that the first fiber to break i_{first} is the fiber with the smallest threshold value

$$i_{\text{first}} = \underset{i}{\operatorname{argmin}}(\sigma_i^{\text{th}}). \tag{20}$$

After the first failure, the order of breaking is not solely dependant on the threshold value. As shown in figure 2.11 bundle B, fiber 3 breaks before fiber 4 despite fiber 4 being weaker. This is because the condition for a fiber breaking, $\sigma_i \geq \sigma_i^{\text{th}}$, is dependant on σ_i, which in turn is dependant on the sate of the fibers. If we instead use that $\sigma_i = \sigma\hat{\sigma}_i$, see equation (8), we can obtain a different condition that is

dependant on σ:

$$\sigma_i \geq \sigma_i^{\text{th}} \implies \sigma \geq \frac{\sigma_i^{\text{th}}}{\hat{\sigma}_i}. \tag{21}$$

This condition is much more useful for our needs since unlike σ_i, σ is one of our control variables. Thus finding the next fiber to break i_{next} can now be calculated by

$$i_{\text{next}} = \underset{i}{\text{argmin}}(\frac{\sigma_i^{\text{th}}}{\hat{\sigma}_i}). \tag{22}$$

In summary, for the purposes of simulation, we mostly care about the order in which to break the fibers, and in finding it, we also find the force required to break each fiber. The order can be determined by σ_i^{th} and $\hat{\sigma}_i$ using equation (22). The threshold values are randomly chosen, so the remaining task is to calculate $\hat{\sigma}_i$. How this is done in the simulation is described in section 3.1.1.

2.7 Additional Terminology

We have introduced many terms and concepts while explaining the FBM and introducing CLS, but there are a few more that need to be presented in order to follow the analysis and discussion of the simulation results.

2.7.1 Critical Strength

The critical strength of a bundle σ_c is the maximum of σ during the breaking process of a bundle. The number of broken fibers k that this occurs at is called k_c. This is an important point from a physical/engineering perspective because from here on, the bundle usually breaks catastrophically all at once. When observing a real breaking process, σ_c is often where the material suddenly snaps. This is not the case for a piece of chewing gum, but most brittle materials will for all intents and purposes snap as soon σ_c is reached.

2.7.2 Avalanches

An avalanche occurs when one or more fibers break at a lower load than the load reached at a previous breaking event. Looking at plot B in figure 2.2 we can see a small avalanche starting around $x = 0.4$. One of the reasons avalanches are interesting is because they are observable in experiments as acoustic emissions, creating a direct way to compare the theoretical model with real materials [21, 22]. This thesis has not considered avalanches in the analysis of the FBMs, but we will take

some time here to discuss them despite their lack of relevance to future discussion because of how important they are in the field of FBMs.

2.7.3 Avalanches - Evidence of Fiber Bundle Mechanics in Experiments

Self-organized criticality was proposed as an explanation for the ubiquitous presence of $1/f$ noise in 1987 [23]. It was proposed that many systems naturally evolve towards points of extreme instability, before eventually collapsing back to equilibrium in a scale free event. In terms of avalanches in a fiber bundle, it means that when an avalanche occurs, the number of fibers in the avalanche could be as few as a single fiber, or comparable to N, regardless of how large N is. In ELS, the number of avalanches $D(\Delta)$ of size Δ has been analytically proven [24] to scale as

$$\frac{D(\Delta)}{N} \propto \Delta^{-5/2}. \tag{23}$$

This analytical result was found using only a single general assumption, that the macroscopic force of the bundle has a single parabolic maximum, meaning that the equation holds for almost all distributions of fiber thresholds. Since ELS works completely independently of the geometry of the fibers in the bundle, this result also holds for bundles of any dimension. Research on avalanche size distributions has found this exponent $\tau^{\text{ELS}} = -5/2$ in multiple other models. The exponent was found very convincingly in a 2D LLS model [25], a soft clamp model [17] and even in a 2D random fuse model (RFM) [26]. Just how universal is this exponent? Might it somehow appear or play a role in real materials as well? Several experiments [27–29], including a FBM simulation [19], have been performed exploring the distribution of crack front propagation velocities when pulling apart slides of glass that have been glued together, all finding an exponent of -2.55, very close to τ^{ELS}. Is this related to τ^{ELS}, and evidence of the ELS FBM modeling the real world, or just a coincidence? There is no shortage of results, both numerical and experimental that find differing exponents where one might expect to find τ^{ELS} [21, 22, 30–33], so clearly there is a limit to the exponents universality, but comparing numerical models to experimental results can be tricky. Perhaps the exponent is hidden behind some transformation that is required in order to justifiably compare avalanche size to real world observables such as crack velocity, number of acoustic emissions per distance, or other measurements that have been used to find power laws. Hansen also shows that if the bundle were to be broken in step wise increments, as opposed to continuously, the exponent is no longer $-5/2$, but -3 [3]. This is an additional complication to comparisons. We believe that despite many experiments finding other exponents, τ^{ELS} could still play some fundamental role in failure, but be hidden and distorted by other effects. The experiments observing the propagation

of a fracture front through glued pieces of glass are especially supportive of the presence of some sort of τ^{ELS} exponent.

It should be noted that the FBM is seldom used for analysing experimental data and that modern acoustic emissions analyses [34–37] often rely on variations of the the Paris-Erdogan crack propagation law [38] developed around 1963, well before the FBMs rise in popularity. The FBM provides a way to understand fracture and failure on a fundamental level, it is not meant to be used on experimental data. The FBM model possesses a valuable attribute by successfully capturing important phenomena like avalanches and 1/f noise through its simple and analytically solvable approach. This combination of a straightforward model replicating intricate behaviors offers practical utility in understanding the rules behind the behavior. The FBM model's ability to provide insights into these complex behaviors underscores its inherent value, despite lacing in direct practical use cases.

2.7.4 Localization

Localization is an event which occurs in the vast majority of LLS and CLS bundles. As a cluster grows, so too does the load on its perimeter. A fiber with a higher load is more likely to break than a fiber with less load. It follows that large clusters grow more quickly than small clusters, creating a positive feedback loop. Once a cluster grows to a certain size, we say that the breaking localizes in said cluster. The other cluster stop growing and *almost* all future breaking occurs on the perimeter of the largest cluster. To demand that *all* future breaking should occur on the largest cluster is too strict and excludes many bundles that should be considered in the localization regime. If all future breaking occurs next to one cluster, the derivative of its size s with respect to the number of broken fibers k will be 1. In this thesis, despite being strict, we say that localization occurs at the first point where

$$\frac{\partial s_{\max}}{\partial k} \geq 1, \tag{24}$$

where $s_{\max}$ is the size of the largest cluster in the bundle. We could choose a smaller value as a criterion for localization, but it then becomes an arbitrary choice, which we ideally want to avoid. For reference, figure 2.17 shows the plot of $s_{\max}$ for various disorders. Note that the slope is usually greater than one, since a cluster can grow at a higher rate when merging with other clusters.

2.7.5 Spanning Cluster

We say that the length of a cluster l is the larger of the width and height of the cluster. A spanning cluster is a cluster where $l \geq L$. Unlike avalanches that can be heard [22] or critical strength that can be seen as the material fails, there is

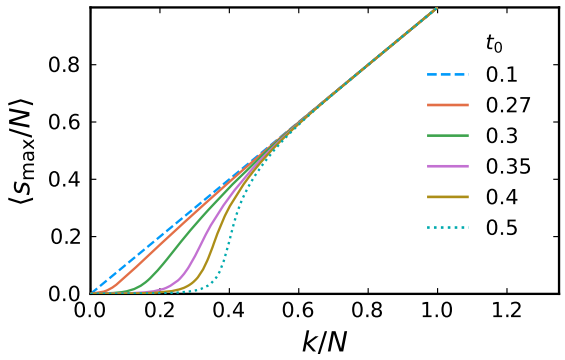

Figure 2.17: Plot of $s_{\max}$ for various disorders.

no physical analogy to a spanning cluster. Spanning clusters are not interesting themselves, but large clusters give better geometrical measurements, and we argue that clusters can not become larger than spanning clusters before starting to grow in unphysical ways. Figure 2.18 shows a bundle that has been tiled in a 2×3 gird, but due to periodic boundary conditions, this grid extends infinitely in the 2D plane and we are only showing a small subsection. Before a cluster is spanning, each cluster has a finite size, such as the light blue, second largest cluster in the figure. However, once a cluster is spanning, there is a chance that it becomes infinitely large, as we see has happened with the red cluster in the figure. Since it connected with itself in the horizontal direction, it has become infinitely wide. We use periodic boundary conditions to center the cluster and not deal with edge effects, but we can not allow non-planar interactions, such as opposite ends of the same cluster meeting. In order to prevent such interactions, we never use clusters where $l \geq L$ for analysis. As soon as the cluster reaches a length of L or greater, we consider the cluster as it was at the previous value of k. This will often result in the length of the cluster being $l = L - 1$, but since a cluster could in theory connect with another cluster of equal size, its length could be as small as $l = L/2$.

For future work, it could be possible to check whether or not a cluster has connected with itself or not, allowing clusters where $l > L$ to be used so long as the cluster is planar. However, if doing so, keep in mind that this could have unintended effects. Two clusters A and B of the same size l_{A} and l_{B}, might behave differently if grown in bundles of differing system size, $L_{\mathrm{A}} \neq L_{\mathrm{B}}$. Depending on what properties you measure, this could potentially have unintended effects that are difficult to notice.

2.7.6 Center of Mass

Finding the center of mass (cm) of a cluster can be a bit tricky. To calculate a cm, we take an average of all the positions of the broken fibers in a cluster. In

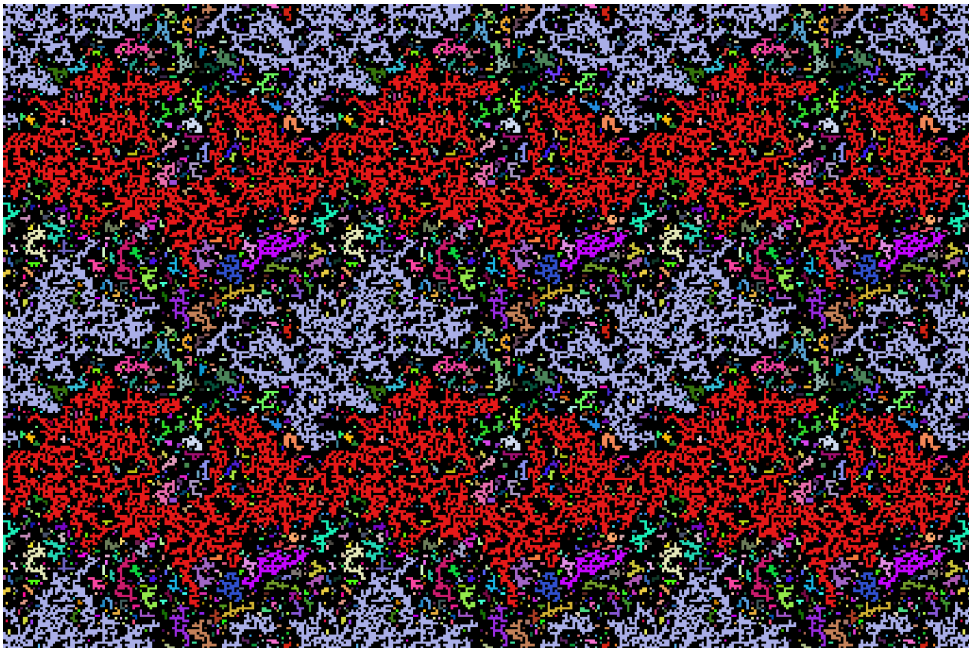

Figure 2.18: A LLS $L = 128$ bundle with a spanning cluster tiled in a 2×3 grid.

other words, we assume that each fiber weighs the same amount. The problem is made apparent in bundle A in figure 2.19. If we naively take the average coordinate position of each fiber in bundle A, we end up with a cm in the middle of the bundle, indicated by a cross, that is quite obviously wrong. Instead what we need to do is keep track of the relative position of each fiber as we explore the cluster, and take an average of the relative positions. See section 3.1.1 for details on how we explore a cluster. Unfortunately, if the cluster is connected to itself such as it is in bundles B and C, this will also lead to ambiguity, and the only way to truly know what the correct center of mass is, is by knowing the prior states of the bundle. This is the reason why we never consider spanning clusters. If there is a connection between the two halves in bundle B, we might end up with the wrong cm, but so long as there is no connection, we always find the correct cm. One could argue that they are both valid center of masses, so does it really matter which one we choose? Yes, in some cases, it does matter what cm we use, for example when calculating the *radius of gyration*.

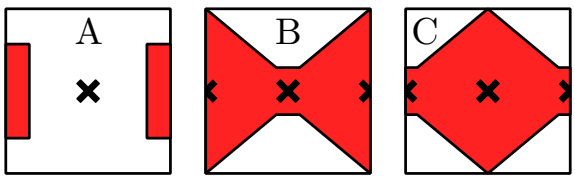

Figure 2.19: Illustrative bundles with crosses marking the center of mass of the cluster.

2.7.7 Radius of Gyration

The radius of gyration is more commonly used to describe how easily an object can spin around an axis through its cm, but for our purposes it will be used in a purely geometrical sense to say something about how large the cluster is, which in turn will later be used to determine the dimensionality of the clusters [39]. The radius of gyration $R_{\mathcal{J}}$ is defined as

$$R_{\mathcal{J}}^2 = \frac{\sum_{j \in \mathcal{J}} r_j}{s_{\mathcal{J}}} \tag{25}$$

where we here let $\mathcal{J}$ also be a set of all fibers j in cluster $\mathcal{J}$ and let r_j is the distance between fiber j and the cm of the cluster. The size $s_{\mathcal{J}}$ also gives a description of how large the cluster is, but $s_{\mathcal{J}}$ cannot distinguish between a sparse or dense cluster, $R_{\mathcal{J}}$ can. This is illustrated in figure 2.20 where bundle 2.20a has a spanning cluster A with fewer broken fibers s_A, but a larger radius of gyration R_A than the spanning cluster B in bundle 2.20b, which has more broken fibers s_B and a smaller radius of gyration R_B, i.e. $s_A < s_B$ and $R_A > R_B$. If we now return to bundle B and C in figure 2.19, we see that bundle B will have a larger radius of gyration compared to bundle C, despite the two bundles being identical apart from the location of the cm.

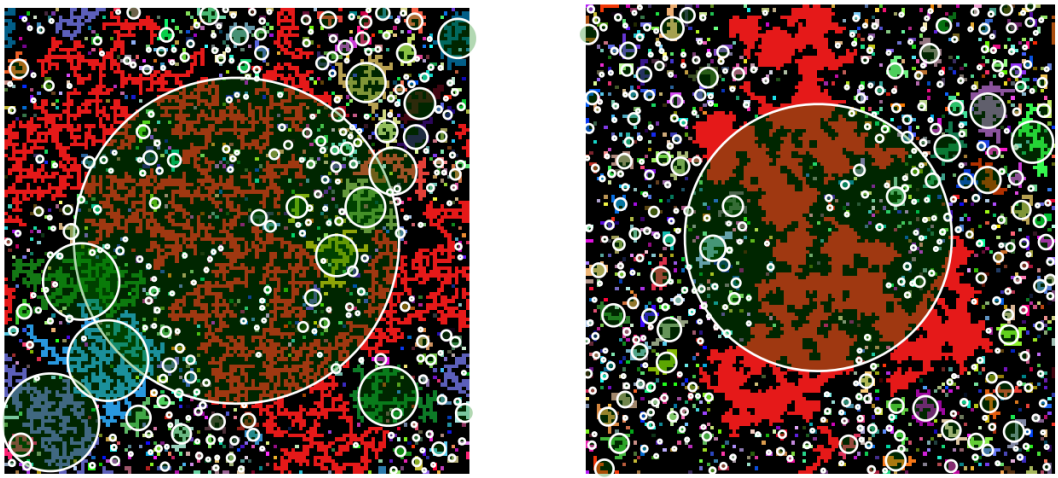

(a) A LLS bundle with a red spanning cluster A of size $s_A = 3006$ and $R_A = 45$.

(b) A CLS bundle with a red spanning cluster B of size $s_B = 3019$ and $R_B = 37$.

Figure 2.20: Bundles where each cluster has its radius of gyration drawn centered on the cm of the cluster.

3 Method

The code used for the simulations is written in Julia.1.7.2 and can be found at https://github.com/EliasL/FiberBundle. Only a small fraction of the code is responsible for breaking the bundle. Approximately 50% is code for making plots and 40% is for data management. This section will only be discussing and explaining the remaining 10% found in "buringMan.jl"[2] which contains the code responsible for the breaking simulation and uses the "burning" algorithm to find clusters in the bundle. Instead of simply starting at the top of this file and explaining what each part does, we will take a more chronological approach, starting with the parts that were developed first until we have a minimal working example of sorts. For a softer start, we recommend anyone writing their own version to start of with a one dimensional version to get some experience with the general idea of the simulation. That being said, this section only covers the implementation of a two dimensional FBM.

3.1 Minimal Working Example

We start of with three arrays $\bar{\sigma}, \hat{\bar{\sigma}}$ and $\bar{\sigma}^{\text{th}}$. Both $\bar{\sigma}$ and $\hat{\bar{\sigma}}$ are arrays of length N containing the load and relative load of each fiber respectively, and $\bar{\sigma}^{\text{th}}$ is an array of length N containing the threshold values of each fiber. Where we previously used σ_i^{th} to refer to the threshold value of fiber i, we now let it also refer to the i-th element of the array $\bar{\sigma}^{\text{th}}$. We do similarly for the other variables:

$$\bar{\sigma} = \overbrace{[0, \cdots, \sigma_i, \cdots, 0]}^{N} \tag{26}$$

$$\hat{\bar{\sigma}} = \overbrace{[1, \cdots, \hat{\sigma}_i, \cdots, 1]}^{N} \tag{27}$$

$$\bar{\sigma}^{\text{th}} = \overbrace{[0.245, \cdots, \sigma_i^{\text{th}}, \cdots, 0.078]}^{N} \tag{28}$$

As discussed in section 2.6, in order to simulate the bundle, we only need the order of the fibers breaking. Our task becomes finding the relative load $\hat{\sigma}_i$.

3.1.1 Calculating Relative Load

Say we have some bundle with k broken fibers. We are given a state array $\bar{S}$ describing the bundle, consisting of only ones and zeros. Zero if the fiber is broken, one if it is not broken. For simplicity, let us stick to the familiar LLS. Looking back

[2] I somehow misheard the name of the algorithm as "burning man", instead of just "burning", and have for the past two years been convinced that the algorithm was somehow related to a burning man.

to equation (9), the expression for $\hat{\sigma}_i$ for a single cluster in LLS, we need to find the size $s_{\mathcal{J}}$ and perimeter length $h_{\mathcal{J}}$ of all the clusters in the bundle. This is where the burning algorithm comes in. The burning algorithm follows these steps

1. Find a broken fiber.
2. Explore all adjacently broken fibers with a flood algorithm.
3. Update load on the perimeter of the cluster.
4. Repeat steps 1-3 until all fibers have been checked.

Figure 3.1 gives a visual explanation of how the algorithm works. We search until we find a broken fiber, illustrated in the left grid. We explore all neighbouring broken fibers with a flood fill, illustrated in the middle grid. After having identified the outline of the cluster, marked with orange, we update the stress of these fibers and continue searching until we reach the next broken fiber or reach the end of the bundle, illustrated in the right grid. The two crosses in the middle grid are put there to emphasize that these fibers will receive additional stress twice, once from each cluster.

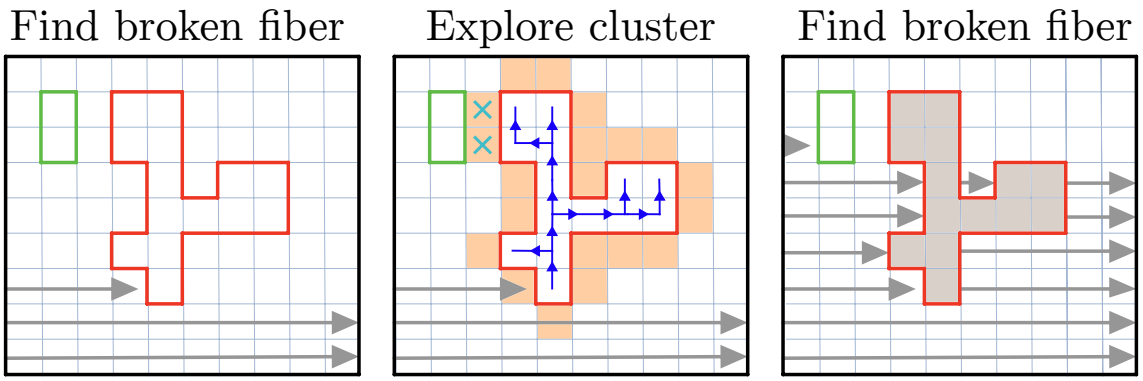

Figure 3.1: A visualization of the burning algorithm. There are three depictions of the bundle in different states of the algorithm. There are two clusters depicted with the colors green and red. The fibers inside of these two shapes are broken, all the other fibers are intact. The grey arrows represent the for loop in algorithm 1. The blue lines represent the flood fill while loop in algorithm 2. The orange line represents the contents of the outline array $\bar{O}$. The two light blue crosses mark fibers that will receive load from both the green and the red cluster.

What follows is a written explanation and pseudo code, but keep in mind that as this is a thesis on physics, not computer science, many details are omitted. As we explore the bundle, we use a cluster id variable c to keep track of which cluster we are currently exploring, and how many clusters there are in total. Referring

back to our visual example in figure 3.1, the red cluster would receive id $c = 1$ and the green would receive id $c = 2$. As we explore the fibers, we use the state array $\bar{S}$ to determine what operation to perform for each fiber. An overview of the possible states can be found in table 3.1. The difference between states -2 and -3 may perhaps be confusing, but in order to handle fibers adjacent to two different clusters, we need to distinguish between the perimeter of the cluster that we are currently exploring and the perimeter of clusters that we have explored earlier.

Table 3.1: Status values of fibers

	Value S_i	Description
Broken	$S_i > 0$	Belongs to cluster S_i
	0	Unexplored fiber
Intact	-1	Unexplored fiber
	-2	Current perimeter
	-3	Past perimeter

Algorithm 1 describes the top level of the burning algorithm. Note that a real implementation will requite additional arguments in the functions. Keep also in mind that this algorithm should be written in such a way that allocations only occur once per bundle. This can greatly speed up computation time.

Algorithm 1 Burning

```
1:  c ← 0                                              ▷ Current cluster id
2:  Ō ← [0 ··· 0]                                      ▷ Outline of a cluster, Length N
3:  for i = 1 to N do                                  ▷ Loop over all fibers
4:      if S̄[i] = 0 then ▷ 0 translates to an unexplored broken fiber. See table 3.1.
5:          c += 1                                     ▷ Increase the cluster id
6:          S̄[i] ← c                                   ▷ Assign this fiber to be part of cluster c
7:          exploreClusterAt(i)
8:          updateOutlineStress()
9:      else
10:         pass                ▷ We ignore fibers that are intact or already explored
```

Algorithm 2 uses a non-recursive flood fill algorithm to explore the cluster. Note that the checkNeighbours function in line 8 modifies $\bar{U}$.

Algorithm 3 starts to fill in some values for s and h by iterating of the neighbours of $currentFiber$. We will later suggest a method for finding the adjacent neighbours, but any method will work.

Take a closer look at line 11. Understanding this line is integral for understanding our implementation. $\bar{O}$ is an array that we want to fill with different numbers i where

Algorithm 2 exploreClusterAt(i)

1: $nrExplored \leftarrow 0$
2: $nrUnexplored \leftarrow 1$
3: $\bar{U} \leftarrow [0 \cdots 0]$ ▷ Unexplored fibers, Length N
4: $\bar{U}[nrUnexplored] \leftarrow i$ ▷ Seed the array with starting point
5: **while** $nrUnexplored > nrExplored$ **do**
6: $nrExplored \mathrel{+}= 1$
7: $currentFiber \leftarrow \bar{U}[nrExplored]$ ▷ This assumes 1-indexing in arrays
8: $nrUnexplored =$ checkNeighbours($\bar{U}, currentFiber, nrUnexplored$)

each i represents a fiber. By doing this, we could for example obtain the total stress around a cluster outline using sum($\bar{\sigma}[\bar{O}]$) where $\bar{O}$ is a vector of indices such that $\bar{\sigma}[\bar{O}]$ is a subset of $\bar{\sigma}$. h is an array of perimeter lengths, so that if we ask "how long is the perimeter of cluster c?" $h[c]$ gives the answer. That is, it is only true once the algorithm has completely explored cluster c, and in algorithm 3, we are in the middle of exploring. As we see in the line just above, line 10, $h[c]$ is continuously being incremented, and is therefore ideal for use in indexing our outline array $\bar{O}$.

Algorithm 3 checkNeighbours($\bar{U}, currentFiber, nrUnexplored$)

1: **for** n **in** neighbours of $curentFiber$ **do**
2: $status \leftarrow \bar{S}[n]$
3: **if** $status = 0$ **then** ▷ 0 translates to an unexplored broken fiber. See table 3.1.
4: $nrUndexplored \mathrel{+}= 1$
5: $\bar{U}[nrUnexplored] \leftarrow n$ ▷ Add neighbour to unexplored
6: $\bar{S}[n] \leftarrow c$ ▷ Update state of neighbour to be part of cluster c
7: $\bar{s}[c] \mathrel{+}= 1$ ▷ Add one to cluster size
8: **else if** $status = -1$ **or** $status = -3$ **then** ▷ If fiber is alive and not added
9: $\bar{S}[n] \leftarrow -2$ ▷ Set neighbour to current perimeter
10: $\bar{h}[c] \mathrel{+}= 1$ ▷ Add one to perimeter length
11: $\bar{O}[h[c]] \leftarrow n$ ▷ Add the neighbour to the outline array
12: **else**
13: **pass** ▷ $status$ should be -2, otherwise something is wrong
return $nrUnexplored$

In algorithm 4 we pass though all the fibers in the perimeter $\bar{O}$ of the current cluster c and add an appropriate amount of stress to the $\bar{\sigma}$ array. Note that we can reuse the array $\bar{O}$ for multiple values of c without resetting it since we only ever use the overwritten part from 1 to $h[c]$.

Algorithm 4 updateOutlineStress()

1: $addedStress = \bar{s}[c]/\bar{h}[c]$ ▷ From eq. 9
2: **for** $i = 1$ to $\bar{h}[c]$ **do**
3: $\quad\bar{\sigma}[\bar{O}[i]]$ += $addedStress$ ▷ Add stress to each fiber in outline
4: $\quad\bar{S}[\bar{O}[i]] = -3$ ▷ Set to past perimeter
return $nrUnexplored$

3.1.2 Finding Neighbours

Algorithm 3 loops over the neighbours of a fiber and we mentioned that we would take a look at one way to find these neighbours. We suggest using a lookup table $\bar{\bar{A}}$ that is precomputed ahead of the breaking process. In other words, it is a $N \times 4$ matrix where each row represents a fiber and each column represents the 4 neighbours of that fiber in no particular order. The table $\bar{\bar{A}}$ can be generated in two passes, we first generate each column i with the entries

$$\tilde{\bar{\bar{A}}}_{i,:} = \begin{bmatrix} i+L \\ i-L \\ i-1 \\ i+1 \end{bmatrix}, \tag{29}$$

where the colon in $\tilde{\bar{\bar{A}}}_{i,:}$ indicates looking at the all the elements in the i-th column. We require a second pass before we arrive at $\bar{\bar{A}}$, but let us look at what we have so far. In order to make sense of these entries, it is useful to reference a numbered grid as in figure 3.2. Take for example fiber $i = 5$. Using equation (29) we find it's neighbours to be 8, 2, 4 and 6, since $L = 3$.

The second pass is needed to deal with the neighbours of fibers on the border of the system. The common solution is to use periodic boundary conditions such that the neighbours of fiber 1 are 4, 7, 3 and 2. The second pass consists of a series of if statements testing for the various possible cases that could occur and gives rise to periodic boundary conditions, see equations 30-33.
For those unfamiliar with mod1 (short for modulus1), it is a function that is very useful when dealing with 1-indexed arrays. Where $\text{mod}(0, L) = \text{mod}(L, L) = 0$, $\text{mod1}(0, L) = \text{mod1}(L, L) = L$. If we check $i = 1$ we see that it fulfills the conditions for equation (31) and (32). Following equation (29) $\tilde{\bar{\bar{A}}}_{1,2} = -2 \rightarrow \tilde{\bar{\bar{A}}}_{1,2} + N = 9 - 2 = 7$ and $\tilde{\bar{\bar{A}}}_{1,3} = 0 \rightarrow \tilde{\bar{\bar{A}}}_{1,2} + L = 0 + 3 = 3$ which is what we expected.

3.2 Data Storage

We want to dedicate a short section for describing how the data storage and processing was handled. There are advantages and disadvantages of our implementation,

1	4	7
2	5	8
3	6	9

Figure 3.2: A $L = 3$ grid with numbered cells.

$$\bar{\bar{A}}_{i,1} = \begin{cases} \tilde{\tilde{A}}_{i,1} - N, & \text{if } i > N - L \\ \tilde{\tilde{A}}_{i,1}, & \text{else} \end{cases} \tag{30}$$

$$\bar{\bar{A}}_{i,2} = \begin{cases} \tilde{\tilde{A}}_{i,2} + N, & \text{if } i \leq L \\ \tilde{\tilde{A}}_{i,2}, & \text{else} \end{cases} \tag{31}$$

$$\bar{\bar{A}}_{i,3} = \begin{cases} \tilde{\tilde{A}}_{i,3} + L, & \text{if mod1}(i, L) = 1 \\ \tilde{\tilde{A}}_{i,3}, & \text{else} \end{cases} \tag{32}$$

$$\bar{\bar{A}}_{i,4} = \begin{cases} \tilde{\tilde{A}}_{i,4} - L, & \text{if mod1}(i, L) = L \\ \tilde{\tilde{A}}_{i,4}, & \text{else} \end{cases} \tag{33}$$

and we will give some advice on what worked and what should be avoided. It is common to break a large number of bundles and only store the averaged quantities after the run is performed. This has the advantage that it is simple and requires little storage space. The disadvantage is that if you later want to obtain a quantity that you did not average over, you would need to run the simulation from scratch. It would be better if you could store all the data you generated, but this quickly becomes too large to handle. If one were to store the force of every fiber in every step in every bundle, it quickly becomes very large. Say that we have 200 bundles of size $L = 512$. If each number is 4 bytes, the data from 200 bundles of just one quantity would be $L^2 \times L^2 \times 200 \times 4\text{B} = 54\text{TB}$. What one could instead do is store the breaking sequence of the bundle. If we know in what order to break the fibers, we can very quickly recreate any state of the bundle and calculate additional properties afterwards. If we are only interested in the properties of a cluster up to where a cluster starts to span the system, we can do this and later resume the progress if we later realize we need to completely break the bundles. The breaking order of 200 $L = 512$ bundles would only take $L^2 \times 200 \times 4\text{B} = 209\text{MB}$. We believe it can be a good idea to store the breaking order, but it is still to slow to effectively work with. In addition to the breaking order we recommend storing several other properties and keeping one section of averaged numbers and one section of individual bundle properties in your storage system. Table 3.2 gives an overview of the properties that were useful to us. The averaged properties would be stored in the averaged storage *and* the bundle specific storage, but the bundle specific properties are pointless to average over, and so they should not be stored in the average storage.

Simulation time is a useful property to average over because if you first perform a simulation on a small number of bundles, you can very accurately estimate the time a future larger simulation will take. This can be useful if the computer cluster is

often busy and prioritizes shorter jobs, but also to quickly get some idea of whether the simulation will finish in a reasonable amount of time. If you schedule a large simulation it would be useful to know if it will take two or four weeks. **Most stressed fiber** is an array where at each step k in the breaking process the fiber with the lowest $\sigma_i/\hat{\sigma}_i$ value (see sec. 2.6) is recorded in position k. **Most most stressed fiber** is the largest value of the most stressed fiber array, and **most most stressed fiber step** is the index of said value. It is useful to split up some of these important single numbers to avoid spending a lot of time getting them later while plotting. **Elongation** is how stretched the bundle is. This enables us to recover relative load via equation (8). **Nr. of clusters**, **largest cluster** and **largest perimeter** are arrays where the appropriate property is calculated for each step k. Next are the spanning versions of cluster size and perimeter. Similar to **most most stressed fiber**, they are the values of **largest cluster** and **largest perimeter** extracted at an particularly interesting k. As the name suggests, the value of k_s is the point at which there exists a spanning cluster. **Spanning cluster step** is just k_s, and we also store the radius of gyration of all the clusters at k_s. Lastly we keep track of the **last step** that has been simulated so that we could resume the simulation at a later time if desired, and the **break sequence** that gives the order of the breaking progress.

Table 3.2: Table of properties to store

	Property	Variable	Size
Averaged	Simulation time		1
	Most stressed fiber	σ	N
	Most most stressed fiber	σ_c	1
	Most most stressed fiber step	k_c	1
	Elongation	x	1
	Nr. of clusters	M	N
	Largest cluster	s	N
	Largest perimeter	h	N
	Spanning cluster size	s	1
	Spanning cluster perimeter	h	1
	Spanning cluster step	k_s	1
	Radius of gyration of spanning step	R	N
Bundle specific	Last step	k	1
	Break sequence	i	N

3.3 Multithreading and Performance

The FBM is well suited for multithreading since it relies on averaging many bundles. If you are comfortable with multithreading in general, giving each thread its own bundle is straight forward. There are possibilities of multithreading inside the bundle, but if you do, you have one less thread that could be used to break a bundle. Julia, the language of our implementation, can optimize and multithread for-loops very easily and will sometimes do so automatically. Because of this, we found, by trail and error, that it was faster to run 50 threads than 64 threads on a 64 core node. Our theory is that the idle cores could help out which ever of the 50 processes needed some assistance dynamically, but multithreading optimization was not a high priority and is therefore not very well implemented or understood.

One way in which multithreading could be implemented in a single bundle is by putting stress calculations into a separate thread. When a cluster is completely explored, a new thread could handle updating the stress of the perimeter of the cluster while the original thread can continue exploring. One could attempt to have multiple exploration treads as well, but because it is very difficult to know if two unexplored clusters are connected, they would need to be merged if two treads realize they are exploring the same cluster. This complication is probably not worth the potential time save, especially since any specialized thread could have been breaking its own bundle instead.

We have not attempted to utilize a GPU for breaking bundles and with our limited understanding of the GPU we think it would be difficult to implement. Perhaps the GPU is suitable for breaking multiple bundles at the same time, as opposed to somehow breaking a single bundle faster, but for larger bundles RAM might become an issue that would at least needed to be worked around.

As a reference for future implementations, our code breaks a single bundle $L = 64$ using LLS on a single threads running on an Intel(R) Xeon(R) Gold 6212U CPU @ 2.40GHz with a real time CPU clock speed of 1000.204MHz in around 0.51 seconds. When using CLS instead of LLS the time increases to 0.62 seconds. The code is written such that all memory allocations occur at the start of the simulation and outside of the breaking process. This is perhaps the most important factor for getting faster code. Memory allocations are not reused between seeds, and while optimizing this could save some time, it only saves time between breaking bundles, and breaking the bundle itself is by far the most time consuming part of the simulation.

4 Results and Discussion

We explore the differences between the CLS and the LLS model using statistical analysis with intermediate interpretation and discussion. Definitions for LLS and CLS are found in sections 2.3 and 2.5 respectively. The threshold distribution used for the fibers in the bundles, unless otherwise specified, is defined by equation (11).

4.1 Geometrical Properties and Morphology

In figures 4.1 and 4.2 we see snapshots of bundles with a range of disorders varying from $t_0 = 0.1$ to 0.5. The snapshot is taken when a cluster in the bundle is spanning the system. Corner Load Sharing bundles focus load onto corners and isolated fibers, because of this, the resulting clusters are dense and less fractal-like than clusters in LLS bundles.

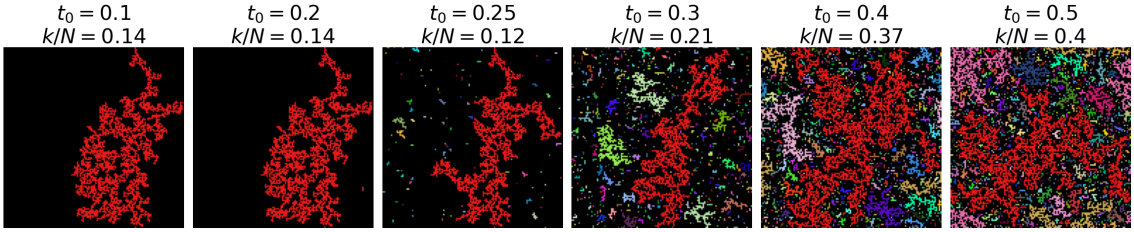

Figure 4.1: Spanning LLS clusters using bundles with a range of disorders.

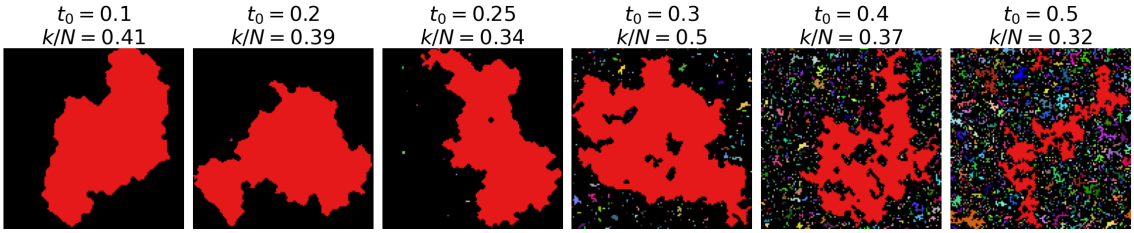

Figure 4.2: Spanning CLS clusters using bundles with a range of disorders.

We can quantify this visual difference by comparing the growth of s and h as a function of the radius of gyration. This rate of growth is effectively the dimensionality (Hausdorff dimension) of the clusters [39]. Figure 4.3 shows how the dimensionality of both the cluster D_s and the perimeter D_h is found for bundles with disorder $t_0 = 0.5$, and table 4.1 gives the number of bundles used for each system size.

Repeating this process for a range of disorders gives us figure 4.4. This provides us with several interesting insights. First, we can observe that as the disorder increases, CLS and LLS seem to approach common values. To explain this, consider a bundle with a large variance in threshold values. As the variance tends towards

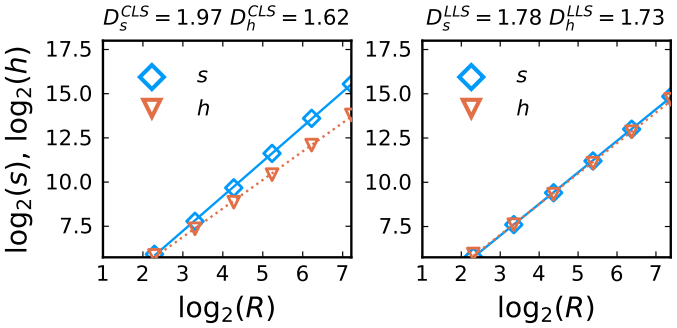

Figure 4.3: Dimensionality of the cluster D_s and the perimeter D_h for the disorder $t_0 = 0.5$, where s is the system size, h is the perimeter length, R is the radius of gyration. The sizes and number of bundles used is provided in table 4.1.

L	Bundles
16	10000
32	10000
64	6000
128	3000
256	1000
512	200

Table 4.1: Number of bundles used in all plots unless otherwise specified

infinity, it means that the distance between any two threshold values will also tend towards infinity. When this is the case, which ever fiber breaks next is unaffected by the presence of clusters and load sharing rules such as LLS and CLS. A finite amount of extra load cannot change the order the fibers break in. In such a scenario, the FBM behaves like *percolation*. Without going into further details about what percolation is, the perimeter of a percolation cluster is believed to be $7/4 = 1.75$ [40, 41], which fits well with our findings: $D_h^{\text{LLS}} = 1.73$, see figure 4.3.

Second, when the disorder is sufficiently low[3], LLS behaves like invasion percolation, a variation of percolation. Invasion percolation has been analytically shown to have a dimensionality of $D_s^{\text{LLS}} = 91/48 \approx 1.89$ [42], which also fits quite well with our result $D_s^{\text{LLS}} = 1.87$, see figure 4.4. Having these two data points supported by existing literature gives credibility to our other data points.

Third, we observe that something interesting happens around $t_0 = 0.25$. Both D_s^{LLS} and D_h^{LLS} are decreasing with increasing disorder. We believe that the cause of the shift in dimensionality is due to other clusters being present during localization. A simple analogy could be to consider a small growing body of water on a glass plate. Under ideal conditions, the body of water would grow uniformly and form a circle around the source of the water. If there were other drops of water already present on the glass, the main body of water would no longer be uniform, but have small bumps where ever a drop recently merged with the main body of water. Hence the dimensionality of the body of water would no longer be two, but slightly less than two. Taking a quick look back at figures 4.1 and 4.2 support this theory.

The CLS dimensionality is especially interesting. Unlike LLS, the dimensional-

[3]We show later that this level of disorder is $t_0 \leq \frac{1}{9}$. See section 4.2.3.

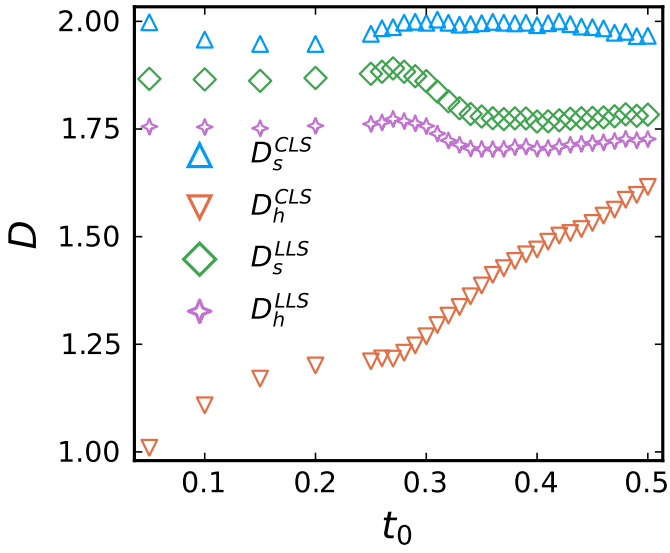

Figure 4.4: Dimensionality of cluster D_s and perimeter D_h for a range of disorders t_0.

ity of CLS seems to vary continuously with disorder. This is quite unexpected and grounds for being sceptical of the result, but the fact that D_s^{LLS} lines up very well with accepted literature gives reason to trust the data. To investigate if the CLS behaviour is real or an artifact of a mistake in the analyses, we calculate the dimensionality again, but using the box counting method [43], see figure 4.5. This result is less convincing for several reasons: D_h^{CLS} is smaller than 1 for $t_0 = 0.05$ and D_s^{LLS} does not match as well with earlier results from literature. Ideally both methods should give the same result, but the discrepancy might be caused by box counting requiring larger system sizes than $L = 512$, or more than 200 samples. That being said, the box counting method does give a slightly less curious behaviour for D_s^{CLS}, and supports the finding that both D_s^{CLS} and D_h^{CLS} vary continuously with disorder.

Although presenting any of these dimensions as accurate would be optimistic, we have two main findings that we want to emphasize: The dimensionality of CLS clusters varies continuously with disorder and there is something occurring around the disorder $t_0 = 0.25$ affecting the dimensionality of both CLS and LLS clusters.

Continuing our investigation into the cause of the dimensionality shift at $t_0 = 0.25$, if the number of preexisting clusters is a factor, we should see some shift in the maximum number of clusters M_{max} around the same disorder. Figure 4.6 shows that M_{max} has an abrupt change around $t_0 = 0.25$, and the change is especially noticeable for LLS bundles. In CLS, the transition seems to sharpen around $t_0 = 0.3$ with increasing system sizes. This is also the disorder where we see D_h^{CLS} start to increase in figures 4.4 and 4.5.

We continue exploring other properties, keeping especially in mind the critical

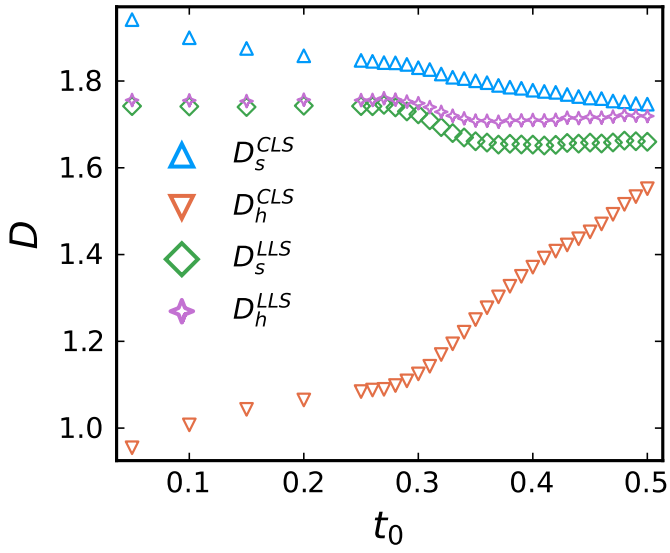

Figure 4.5: Dimensionality of cluster D_s and perimeter D_h for a range of disorders t_0 using the box counting method based on 200 $L = 512$ bundles.

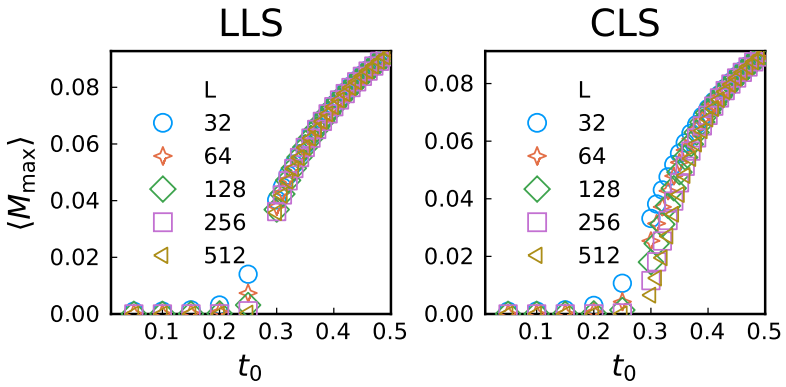

Figure 4.6: Maximum number of clusters over disorder t_0 for several system sizes.

disorder $t_c = 0.25$. The following section investigates how the strength of the bundle behave at these disorders.

4.2 Bundle Strength

The FBM is a statistical model. Most properties we study are averages, and to be clear, an averaged property, for example $\langle \sigma \rangle$, is not averaged over the values of k, but each $\sigma(k)$ is averaged over many bundles. During this process of averaging, we might affect the data in unexpected ways. The maximum strength of a bundle is an excellent example of this, and has also been the topic of a paper by Kjellstadli [44]. We will be considering a similar situation to that discussed by Kjellstadli, but also propose an alternative approach to averaging which may improve the interpretation

of the statistical results.

4.2.1 Max of Averaged Tension

Figure 4.7 shows $\langle\sigma\rangle$ using LLS and CLS, but since the plot using LLS is a bit cluttered, we will focus on the CLS plot. We want to find the critical strength σ_c of the CLS bundle for a given disorder. A reasonable approach might be to take the maximum value of $\langle\sigma\rangle$, but it turns out that making this choice creates some problems. A better approach would be to take the average over σ_c values from individual bundles, and average over many bundles in the end. We want to argue out that

$$\langle\sigma_c\rangle = \langle\max(\sigma)\rangle \neq \max(\langle\sigma\rangle). \tag{34}$$

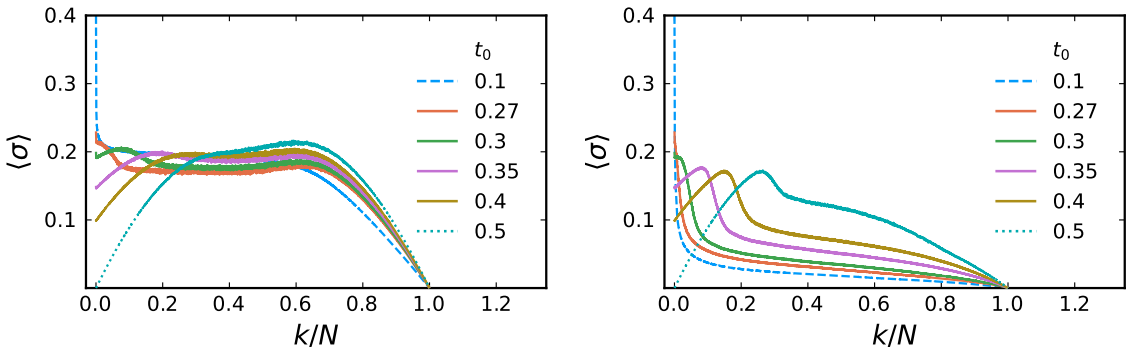

Figure 4.7: The strength of a bundle $\langle\sigma\rangle$ over k/N for several disorders t_0 using LLS (left) and CLS (right). The maxima of the curves shown in these plots do not give a good representation for the value of σ_c

The difference this makes is especially drastic for the LLS model. The two plots to the left in figure 4.8 shows what both σ_c and k_c should look like, and the two plots to the right illustrates the problems that arise when making this averaging mistake.

To illustrate why k_c is larger than the location of the maximum of $\langle\sigma\rangle$, we look at the stress of several bundles that have not been averaged, see figure 4.9. There are large fluctuations in each bundle resulting in solid blocks of color instead of providing useful insight into how the bundle behaves. The natural choice for cleaning up noisy data is to use an average, but note that there is no "noise" here, each value is exactly the correct stress experienced by the bundle. We want to argue that instead of averaging, it is justifiable to use a maximum function that chooses the highest stress value out of each section in a partition of the breaking process. Using a maximal value gives a view of the strength that is more similar to something one would expect from an experiment. We would not be able to measure all the

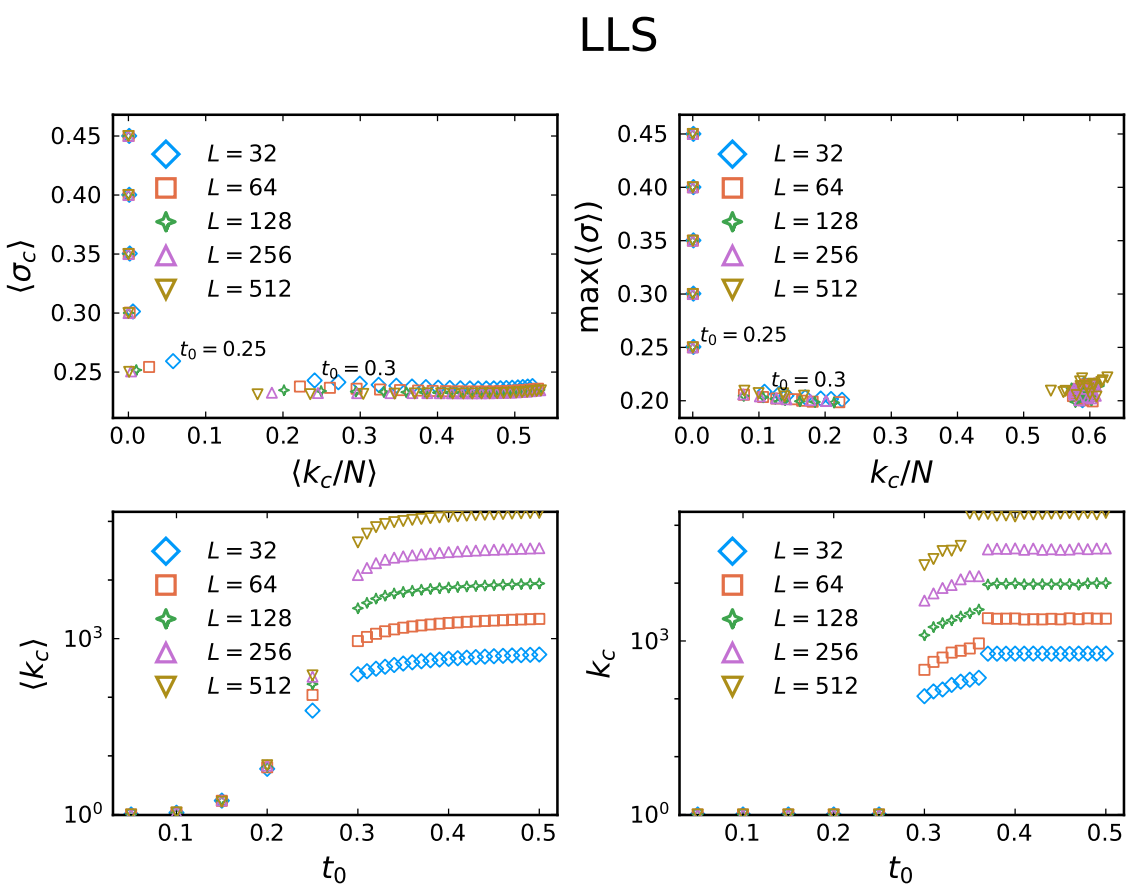

Figure 4.8: Illustration of the difference between two ways to find the critical strength of a bundle. Two points in each of the top plots are labeled with their disorder t_0 to indicate which direction the disorder increases or decreases.

fluctuations from an experiment, and the fluctuations we did manage to measure would come from the strongest configurations. We also challenge the idea of using an average value: imagine stretching a rope. If the strength of the rope was determined by the average strength of the fibers, then adding a weak fiber to the rope would make it weaker. Adding a fiber clearly makes the rope stronger, not weaker! The average strength of the fibers is simply not what we are interested in.

To get a better view of how this bundle might behave in a more realistic environment, we divide the breaking process into 100 sections and only plot the maximum σ value for each section. We call this process $\max(\sigma_{100})$ and use it to make figure 4.10. When we compare the CLS bundles plotted in figure 4.10 with the averaged values in figure 4.7 we notice many similarities, but perhaps most striking is that each bundle individually seems to fall in strength more drastically than the averaged values would suggest. Using this plot, and an illustrative example, we can answer the original question, why is k_c larger than the location of the maximum of $\langle \sigma \rangle$? If we imagine taking the average of only two curves with sharp drops similar to the

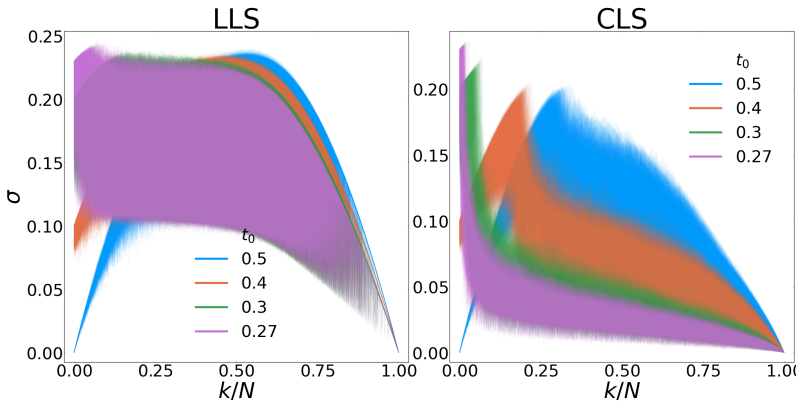

Figure 4.9: The strength σ of 100 bundles of each disorder using a system size of $L = 128$.

ones we see in figure 4.10, it might look something like figure 4.11. Note now that the two critical strengths ${}^{A}\sigma_c$ and ${}^{B}\sigma_c$ occur at $k = 4$ and 2 respectively. It is better, for reasons discussed above, to let $\langle\sigma_c\rangle = (5+6)/2$ and $\langle k_c\rangle = 3$ instead of looking at the averaged value, shown here as a dashed green line, giving $\langle\sigma_c\rangle = 5$ and $k_c = 2$. Applying this reasoning to figure 4.10, it is clear to see that averaging will have a similar effect of both lowering the critical strength value σ_c, as well as moving k_c to a lower value.

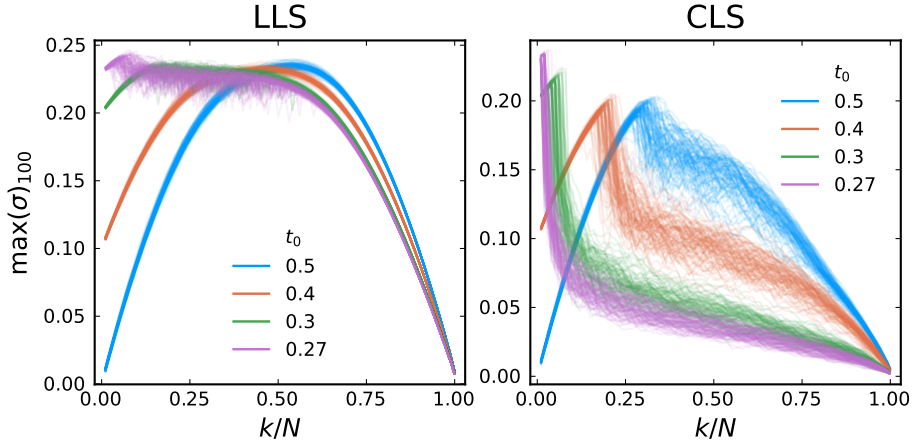

Figure 4.10: The maxed strength $\max(\sigma_{100})$ of 100 bundles of each disorder using a system size of $L = 128$.

4.2.2 Critical Strength and Localization

A paper on crack growth in natural composite materials opens with: "Catastrophic failure of natural and engineered materials is often preceded by an acceleration and localization of damage ..."[32]. Unlike LLS bundles which seems to maintain its

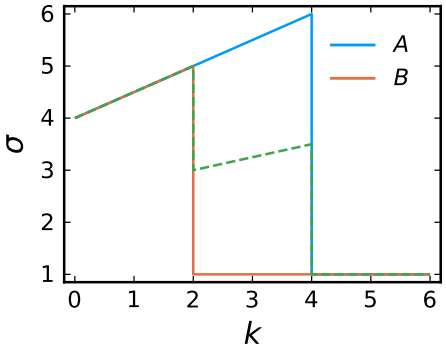

Figure 4.11: A toy example to illustrate the effect of averaging over two curves A and B with sharp drops. The dashed line is the average of A and B.

strength over the majority of the breaking process, CLS bundles seem to reach a critical point and then suddenly loose a large fraction of their strength. How well does localization coincide with the critical strength of CLS bundles? Using the definition of localization from section 2.7.4, we can compare the point of localization k_l to the point of critical strength k_c, see figure 4.12. At low disorder $t_0 < 0.25$ we see that $k_l = k_c$. This is expected since the bundle is so uniform and brittle that at the first few failures, the bundle immediately collapses, setting both $k_l/N = 1$ and k_c/N close to zero. The next region is defined by $k_l > k_c$. This region is much shorter in LLS than in CLS and goes against what we would expect from natural materials, at least according to our quote from the paper [32]. We could "fix" this by setting a leaner definition for localization, instead of demanding a growth rate of 1, we could set it to $\frac{1}{2}$, and to show what this would look like, we have plotted this as $k_l\,(1/2)$. The third region, where $k_l < k_c$ seems to occur around $t_0 > 0.27$ for LLS but not until $t_0 > 0.45$ in CLS. Regardless of whether we use k_l or $k_l\,(1/2)$, they both follow k_c surprisingly closely. Unlike k_l in LLS which separates from k_c around $t_0 = 0.3$, k_l in CLS sticks close to k_c throughout all the disorders that we simulate. This suggests that k_l, perhaps in the form $k_l(1/2)$, could act as a precursor to critical failure.

Following our discovery of how closely k_l follows k_c, we want to see if this behavior exists for bundles with other distributions as well. We test this using the Weibull distribution. The most common parameters for the Weibull distribution are the shape parameter k and the scale parameter λ, but since we already use k, we substitute it with t_w. We set $\lambda = 1$ and run t_w through values from 1 to 5. Note that $t_w = 5$ translates to a low disorder, and $t_w = 1$ translates to a quite high disorder. In fact, the disorder becomes so high, that LLS and CLS both start behaving like percolation, but more on this later. Finally, we scale the distribution so that the mean is always kept at 0.5. Figure 4.13 shows that the point of critical failure k_c

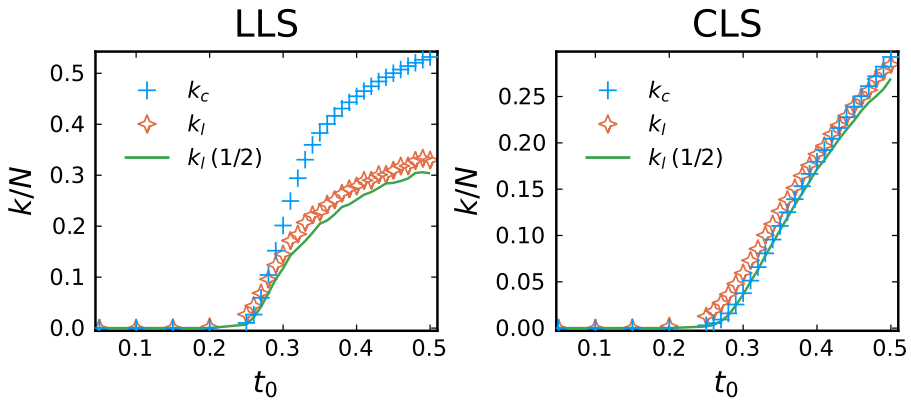

Figure 4.12: The point of critical strength k_c and localization k_l as a function of disorder. We also plot $k_l\,(1/2)$ which uses a growth rate of 1/2 for classification of localization and is plotted as a line instead of markers to give a clearer view of k_c.

is exactly followed by k_l using the Weibull distribution as well! It does so especially well in CLS bundles. Granted, it falls off for very high disorders, but in this regime of disorder, breaking becomes more random and less localized, eventually resulting in percolation.

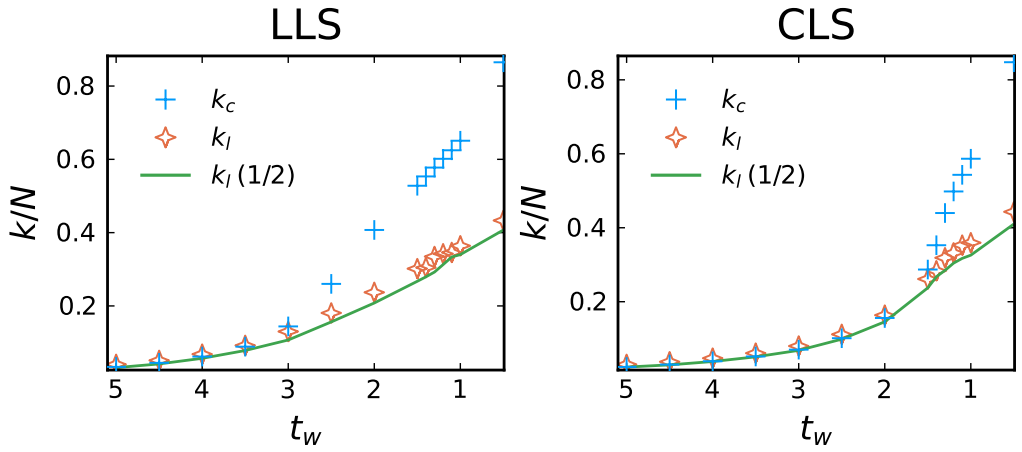

Figure 4.13: The same properties as in figure 4.12. Note that for comparison with figure 4.12, the x-axis has been flipped. The variable t_w is the shape parameter of the Weibull distribution and acts as disorder similarly to t_0.

To illustrate how large the disorder is, we can compare the average strength of the two bundles as shown in figure 4.14. The fact that the curves associated with a disorder of 0.5 are almost identical, despite CLS and LLS behaving very differently for lower disorders, is telling of how large the disorder is, especially since we see no sign of this happening in the same plot using our uniform distribution, see figure 4.7.

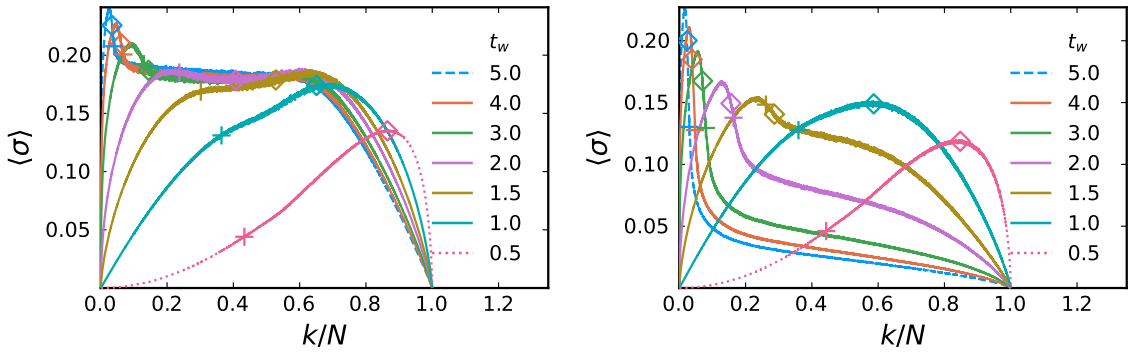

Figure 4.14: Averaged strength $\langle\sigma\rangle$ of LLS (left) and CLS (right) $L = 128$ bundles using the Weibull distribution. Note that $t_w = 5$ translates to low disorder.

4.2.3 Critical Strength Scaling

Another interesting feature of the FBM is critical strength scaling with system size. It is not obvious why there should be a difference between a single rope of "strenght" ten versus ten ropes of strength one, for some definition of strength, but the FBM suggests that there would be a difference. In fact, as the number of fibers in the FBM approaches infinity, the critical strength σ_c of most bundles approaches zero. To see why, we need to add one additional detail: the distribution of load on the ropes is not uniform. If we imagine our rope being divided into 10000 equally strong pieces, each rope will only have a strength of 0.001. If now the load on the ropes is even slightly out of balance, one of the 10000 ropes could easily snap. We should at this point familiar with the effect of load sharing and the consequence a single failure could have on the other fibers. Hansen [3] showed analytically that in the 1D LLS bundle, the critical strength of the bundle scaled as

$$\sigma_c^{-1} \propto \frac{\ln(N^2)}{\ln(\ln(N^2))}. \tag{35}$$

Although this was shown using a first order Taylor series approximation, further investigation showed that a second order approximation gives an exact result (A. Hansen, personal communication, 2022). Note that even though $\lim_{N\to\infty} \sigma_c = 0$, $\lim_{N\to\infty} k_c \neq 0$ but rather $\lim_{N\to\infty} k_c/N = 0$.

Despite some attempts, we have not found a similar scaling in the 2D LLS, and to the best of our knowledge, neither has anyone else, but other models do shown similar scaling. Hidalgo *et al.* [45] using the γ-model, a softer version of LLS, and Biswas *et al.* [46], using a 1D FBM with some tunable range parameter, found that

$$\sigma_c \propto \frac{1}{\ln(N)}. \tag{36}$$

We have found a similar scaling using CLS that closely follows

$$\sigma_c \propto \frac{1}{\ln(\ln(N))}, \tag{37}$$

as shown in figure 4.15. The most interesting details of the figure are found in the inset, where both the slope of the fit, and the deviation from the fit has been plotted. We see that there is a large deviation centered around $t_c = 0.25$, at the same level of disorder as many of our other findings.

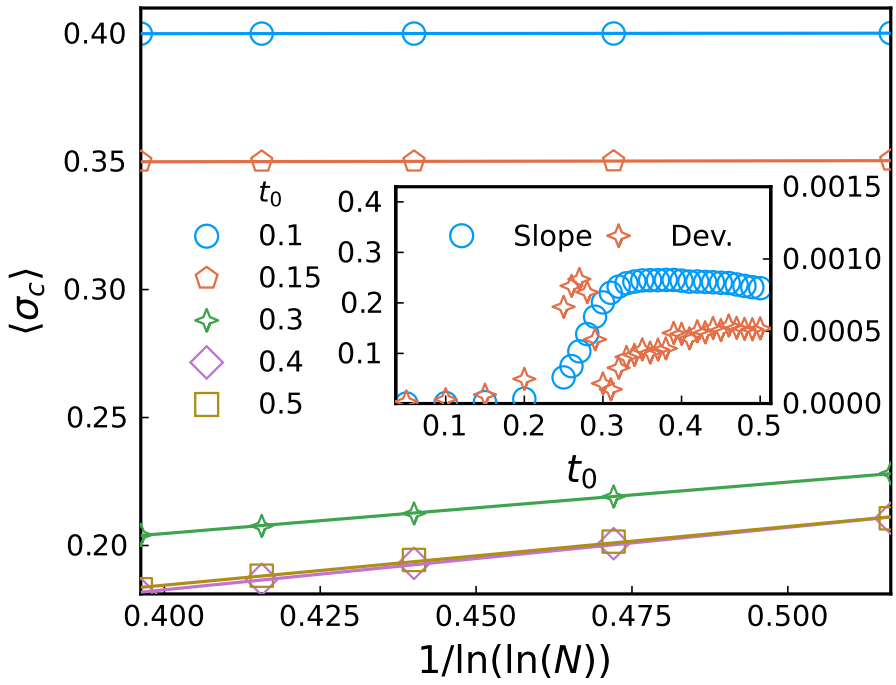

Figure 4.15: The scaling of $\langle \sigma_c \rangle$ as a function N with an inset showing the slope of the fits in the main plot, as well as the deviation from the fits. Sizes used are L= 32, 64, 128, 256 and 512.

To explain why the deviation is large at $t_0 = 0.25$, we also plot $\langle \sigma_c \rangle$ as a function of t_0, see figure 4.16. Let us first start with the ultra-low-disorder, or ultra-brittle region $t_0 \leq \frac{1}{9}$. In this region, bundles reach their critical strength just before the first fiber breaks and their critical strength is therefore determined by the single weakest fiber in the bundle. We can show this quite simply by arguing that the worst case scenario for a complete bundle failure is the situation where the weakest possible fiber is surrounded by four of the strongest possible fibers. If, when the weakest fiber breaks, even the strongest possible fiber breaks as a consequence, then all bundles are guaranteed to fail after the first fiber. We let $W = 0.5 - t_0/2$ be the smallest possible threshold value for a given t_0, i.e. the weakest possible fiber, and $S = 0.5 + t_0/2$ be the largest threshold value, i.e. the strongest. Since the weak

fiber distributes its load equally onto the four surrounding strong fibers (In both LLS and CLS), we require that

$$\frac{5}{4}W = S \tag{38}$$

for the strong fibers to break when the weak fiber breaks. Inserting for W and S we get

$$\frac{5}{4}\frac{1-t_0}{2} = \frac{1+t_0}{2}, \tag{39}$$

which gives

$$t_0 = \frac{1}{9}. \tag{40}$$

This explains why for ultra-low disorders, $\langle\sigma_c\rangle$ does not scale with N: $\langle\sigma_c\rangle$ is always determined by the first fiber. In the low disorder, brittle region $\frac{1}{9} < t_0 < 0.25$, the critical strength is determined by the first few fibers, see the bottom left plot in figure 4.8, but still follows the trend of $\langle\sigma_c\rangle = 0.5 - t_0$ as seen in figure 4.16. Although the critical strength of the bundle is not *guaranteed* to occur at the weakest fiber, it is still very likely, and even more likely to occur after a few hand fulls of fibers, irrespective of system size. This is why $\langle\sigma_c\rangle$ continues to follow the straight line until around $t_c = 0.25$. What happens here is that k_c/N becomes significantly larger, and for LLS, begins to tend towards a fixed value, regardless of system size. Figure 4.17 shows this fraction as a function of t_0 for both LLS and CLS, similar to the bottom left plot in figure 4.8, but scaled with N. CLS seems to maintain some system size dependence in $\langle k_c\rangle$ as it did in $\langle\sigma_c\rangle$, but the spacing seems to decrease slightly for higher values of t_0.

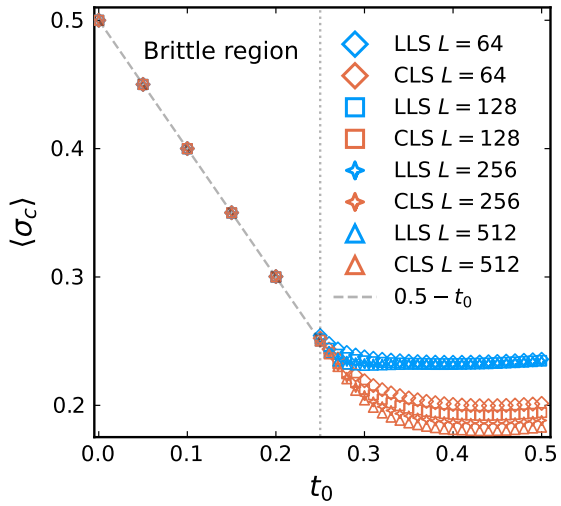

Figure 4.16: The scaling of $\langle\sigma_c\rangle$ as a function t_0 for several system sizes.

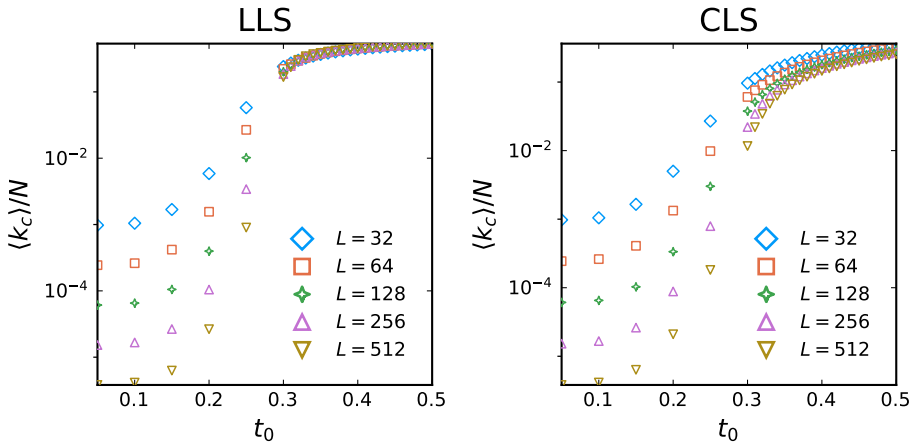

Figure 4.17: $\langle k_c \rangle / N$ over t_0 for several system sizes. Similar to bottom left plot in figure 4.16, but scaled with system size N.

As a small digression, we can take a closer look at this spacing by plotting $\langle k_c \rangle$ in the same way that we plotted $\langle \sigma_c \rangle$ in figure 4.15 to see if the distance between $\langle k_c \rangle / N$ for different system sizes changes as a function of t_0, see figure 4.18. Curiously, the slopes in figures 4.15 and 4.18 are quite similar in shape. This suggests a connection between $\langle \sigma_c \rangle$ and $\langle k_c \rangle$ that may be of interest in further work.

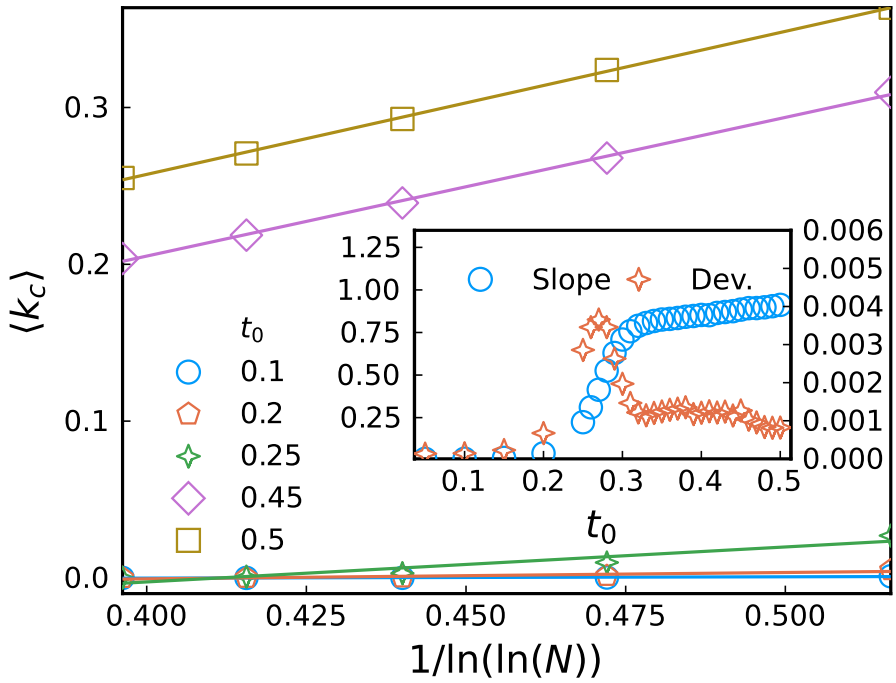

Figure 4.18: The scaling of $\langle k_c \rangle$ as a function N with an inset showing the slope of the fits in the main plot, as well as the deviation from the fits.

Returning to the original question we asked about figure 4.15: Why is there a large deviation from the fit to a straight line around $t_c = 0.25$ for CLS? The reason is that for $t_0 < 0.25$, there is no scaling, the slope is 0, and there needs to be some transition from the brittle, non-scaling region $t_0 < 0.25$ to the non-brittle scaling region $t_0 > 0.3$. This is well illustrated in figure 4.16. At the beginning of the transition, all the points from the different system sizes are all still very close together, and this amplifies any random noise and effects of using small system sizes like $L = 32$ and 64. We believe that the deviation from a line is due to limited sampling and small system sizes and that with larger systems, the deviation could disappear completely.

We end this section with an open question that might be of interest: Why the slopes in the inset in figure 4.15 stop increasing, and even decrease a bit? Does the scaling with N eventually disappear again? A similar trend was seen in the γ model studied by Hidalgo *et al.* [45], but not mentioned in their paper.

4.2.4 Why Is There No Scaling in LLS?

In the process of finding answers, figure 4.16 begs another question: Why is there no scaling in LLS? We have no good explanation, but here is some discussion around the issue. First of all, let us keep in mind the only difference between LLS and CLS: the perimeter of a cluster in LLS receives a uniform load, where as the perimeter of a cluster in CLS does not. The load is distributed less uniformly. We then revisit the example we gave at the beginning of section 4.2.3, and think about which qualities are required for N dependant scaling. In our example, we claimed that the load that each fiber experiences needs to have a non-uniform distribution, but this is not quite true. System scaling also happens in the ELS model due to the non-uniform distribution in the threshold values. Exactly how these two factors, non-uniform load and non-uniform threshold value affect the scaling has not been looked into, but we suspect that the additional variance in the load distribution of CLS bundles creates better circumstances for N dependence, compared to LLS bundles where the load is distributed uniformly around the cluster.

4.2.5 Connection Between Average Threshold Value and the End of the Brittle Region

We want to point our yet another aspect related to the critical strength, and we see this curiosity also best illustrated in figure 4.16. LLS and CLS separate around $t_c = 0.25$, and this just happens to be exactly half of the mean value of the thresholds

$\langle \sigma_i^{\text{th}} \rangle$, i.e.

$$\frac{\langle \sigma_i^{\text{th}} \rangle}{2} = \sum_i^N \frac{\sigma_i^{\text{th}}}{2N} = 0.25. \tag{41}$$

Is this a coincidence? A more refined question is: Why are the bundles brittle until $t_c = 0.25$? We believe that there is a satisfying analytical explanation, and that this might also be related to the explanation for why there is no system size dependant scaling of $\langle \sigma_c \rangle$ in LLS, but these are both left as open questions.

4.3 Choice of Distribution

We briefly explored the use of a Weibull distribution in section 4.2.2 and we want to give some comments regarding choosing a uniform distribution like the one we have mostly used this thesis defined in equation (11), versus using the Weibull distribution, exponential distribution or some other distribution.

4.3.1 Limited Disorder

While using our uniform distribution, the maximum amount of disorder we could get was setting $t_0 = 0.5$. Higher values of t_0 would give negative threshold values, and our code behaved unpredictably when dealing with such threshold values. Using the Weibull distribution provided a much greater capability of creating disordered bundles, and we believe higher values of t_w would be able to create suitable levels of homogeneity as well. Further work should use the Weibull distribution and perhaps other distributions as well, but performing simulations for multiple types of distributions at the same time requires a significant amount of computation time.

4.3.2 Distribution Behaviour?

A question we would be interested in seeing explored in future work is matching the disorder range we explored with the uniform distribution to some range of disorders using the Weibull distribution. If the bundles behave fundamentally different when using the uniform distribution or the Weibull distribution, this might not be possible, but seems for example likely that there should be some region where $\langle \sigma_c \rangle$ is determined by the weakest fiber such that CLS and LLS collapse. This is shown in figure 4.16 in the region $0 \leq t_0 \leq 0.25$. See now the same properties plotted using the Weibull distribution in figure 4.19. Setting $t_w = 5$ is not enough to enter the ultra-brittle region that we have for $t_0 < 0.25$, but we do see that LLS and CLS are converging, perhaps meeting at $t_w = 10$. The question is now, before they converge do we see the same behavior as we see in figure 4.16? Both LLS and CLS have regions, $t_0 > 0.4$ and $t_0 > 0.45$ respectively, where $\langle \sigma_c \rangle$ starts to increase a bit. Will

we see this in when using the Weibull distribution? Or is the behaviour dependant on the distribution? If we adjust our uniform distribution in equation (11) to give even higher levels of disorder, will we start to see $\langle \sigma_c \rangle$ fall as we do in figure 4.19? Looking at the values of $\langle \sigma_c \rangle$ in the two plots, we see that $\langle \sigma_c \rangle$ for $t_0 = 0.5$ using the uniform distribution (fig. 4.16), is smaller than $\langle \sigma_c \rangle$ for $t_w = 5$ using the Weibull distribution (fig. 4.19) for both LLS and CLS. This could mean that there is a local maximum in the critical strength as a function of disorder. If this is the case, it would be very important to understand the underlying mechanisms at play in order to reproduce the effect in materials.

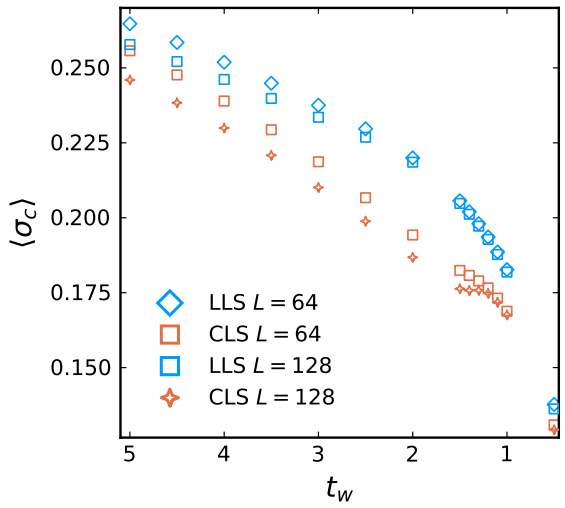

Figure 4.19: The scaling of $\langle \sigma_c \rangle$ as a function t_0 for $L = 128$ and 64. Note that the x-axis has been flipped for comparison with figure 4.16.

5 Summary

5.1 Definition and Implementation of CLS

We began with the introduction of the FBM, ELS, LLS and eventually CLS, a variation of LLS which distributes more load onto fibers with fewer neighbours, i.e. corners. The motivation for this change is that it is more realistic and relatively simple. There are many ways to make the model more realistic, but many of them might only make a negligible difference in results, while introducing a significant amount of complexity. We were interested to see what kinds of new behaviours we might find in CLS, and if they are interesting enough to justify the added complexity. We belive CLS provides many new avenues of research and is well worth the added complexity.

Our implementation uses the burning algorithm and we have included pseudo code for a minimal implementation in section 3.1. The full code is public and available at https://github.com/EliasL/FiberBundle. Averaged data is available in the same repository, but the raw data is only available at insistent request, granted also that we are able to access it when the request is received. The raw data is currently in the PoreLab cluster at NTNU and is too large to conveniently download (762GB).

5.2 Results and Open Questions

We compared the morphology of both LLS and CLS bundles over a range of disorders in section 4.1. Plotting the dimensionality resulted in several notable results, see figure 4.4:

1. Values of D_s^{LLS} for $t_0 = 0.05$ and $t_0 = 0.5$ are supported by existing literature.
2. D_s^{CLS} and D_h^{CLS} vary continuously with t_0.
3. Drastic change in dimensionality around $t_0 = 0.25$.
4. Drastic change in M_{max} around $t_0 = 0.25$.
5. Box counting method plot casts doubt on the behaviour of D_s^{CLS}, see figure 4.5.

We had little success using the box counting method as all our values were warped and in disagreement with known values, see figure 4.5. It did provide a more reasonable behaviour for D_s^{CLS}, but still showed a continuous variation with t_0. The fact that the dimensionality varies continuously, and not in steps as LLS does, is quite curious and a topic for further research.

Next, we wanted to study the behaviour of the bundle strength, keeping in mind that "something" happened around $t_0 = 0.25$. In section 4.2.1 we criticise using an average over bundle strengths and argue that one should use a maximum function instead: A rope does not become weaker by adding a weak thread. Having noted that the CLS bundles have very sharp drops in their strengths, section 4.2.2 investigates whether or not this collapse coincides with localization. We find that k_c and k_l fit very well for CLS even under multiple distribution functions, and especially when using a arbitrarily tuned definition of localization, $k_l\,(1/2)$, see figures 4.12 and 4.13. With better argumentation, it might be possible to find a good definition of localization that behaves like $k_l\,(1/2)$. Section 4.2.3 presents a scaling of the critical strength $\langle\sigma_c\rangle$ as a function of N, see equation (37), also repeated here:

$$\sigma_c \propto \frac{1}{\ln(\ln(N))}, \tag{42}$$

and referenced other models with similar scaling. While the scaling is interesting in it self, we focused our attention on the fact that here too, there is an issue around $t_c = 0.25$: At this disorder, $\langle\sigma_c\rangle$ is less like a straight line than for any other disorder. We argue that the reason for this is because at the beginning of the transition from no scaling to a non-zero scaling, the slope is very sensitive to fluctuations and effects of using small systems like $L = 32$ and 64. This explained the spike in deviation from the fit, but we left why the slopes in the inset began to decrease with higher disorder as an open question. Figure 4.17 shows a very similar scaling, and hints that $\langle k_c\rangle$ might be a useful value to include in further study of critical strength scaling. Section 4.2.4 and 4.2.5 pose two open questions that we suspect may be connected:

1. Why does $\langle\sigma_c\rangle$ not scale with N in LLS?
2. Why does the brittle region stop at $t_0 = \langle\sigma_i^{\text{th}}\rangle/2$?

The last section, section 4.3, discusses issues around the choice of the distribution function. Our work is mainly based on the uniform distribution described in equation (11), and a limitation we ran into using it was its range of disorder. The Weibull distribution is capable of exploring bundles with much greater disorder, and should therefore be used in future work. We also ask if the behaviour of the bundle is dependant on the disorder, but as we only simulated Weibull distributions using $t_w = 0.5$ to 5, we had no overlapping region of disorder to compare with. It seems as though the missing region might contain a local maximum for the critical strength. Understanding the mechanisms that create this potential maximum could be important for creating stronger materials.

References

[1] Yao Tang, Dave H. Chan, and David Z. Zhu. The modeling of free-fall arch formation in granular flow through an aperture. *Frontiers in Physics*, 10, 2022.

[2] A. B. Zolotukhin and A. T. Gayubov. Analysis of nonlinear effects in fluid flows through porous media. *Journal of Petroleum Exploration and Production Technology*, 12(8):2237–2255, 8 2022.

[3] A. Hansen, P.C. Hemmer, and S. Pradhan. *The Fiber Bundle Model: Modeling Failure in Materials*. Wiley, 2015.

[4] J. Williams. Introduction to linear elastic fracture mechanics. *European Structural Integrity Society*, 28:3–10, 12 2001.

[5] R.J.R. Rosa, H.B. Coda, and R.A.K. Sanches. Blended isogeometric-finite element analysis for large displacements linear elastic fracture mechanics. *Computer Methods in Applied Mechanics and Engineering*, 392:114622, March 2022.

[6] M.J. Buehler. Atomistic modeling of materials failure. *Atomistic Modeling of Materials Failure*, pages 1–488, 01 2008.

[7] Oguz Umut Salman, Roberta Baggio, Brigitte Bacroix, Giovanni Zanzotto, Nikolai Gorbushin, and Lev Truskinovsky. Discontinuous yielding of pristine micro-crystals. *Comptes Rendus. Physique*, 22(S3):201–248, December 2021.

[8] Fredrick Thomas Peirce. 32—x.—tensile tests for cotton yarns v.—"the weakest link" theorems on the strength of long and of composite specimens. *Journal of the Textile Institute Transactions*, 17(7):T355–T368, 1926.

[9] Henry Ellis Daniels and Harold Jeffreys. The statistical theory of the strength of bundles of threads. i. *Proceedings of the Royal Society of London. Series A. Mathematical and Physical Sciences*, 183(995):405–435, 1945.

[10] L. de Arcangelis, A. Hansen, H. J. Herrmann, and S. Roux. Scaling laws in fracture. *Phys. Rev. B*, 40:877–880, Jul 1989.

[11] D Sornette. Elasticity and failure of a set of elements loaded in parallel. *Journal of Physics A: Mathematical and General*, 22(6):L243, mar 1989.

[12] Stefan Hiemer, Paolo Moretti, Stefano Zapperi, and Michael Zaiser. Predicting creep failure by machine learning - which features matter? *Forces in Mechanics*, 9:100141, 2022.

[13] Bikas K. Chakrabarti. A fiber bundle model of traffic jams. *Physica A: Statistical Mechanics and its Applications*, 372(1):162–166, 2006. Common Trends in Traffic Systems.

[14] Yingrui Zhang and Osman Yağan. Optimizing the robustness of electrical power systems against cascading failures. *Scientific Reports*, 6(1):27625, Jun 2016.

[15] F. Kun, S. Zapperi, and H.J. Herrmann. Damage in fiber bundle models. *The European Physical Journal B*, 17(2):269–279, 2000.

[16] Achille Capelli, Ingrid Reiweger, Peter Lehmann, and Jürg Schweizer. Fiber-bundle model with time-dependent healing mechanisms to simulate progressive failure of snow. *Physical Review E*, 98(2):023002, 2018.

[17] G. George Batrouni, Alex Hansen, and Jean Schmittbuhl. Heterogeneous interfacial failure between two elastic blocks. *Physical Review E*, 65(3):036126, 2002.

[18] S. Patinet, D. Vandembroucq, A. Hansen, and S. Roux. Cracks in random brittle solids:: From fiber bundles to continuum mechanics. *The European Physical Journal Special Topics*, 223(11):2339–2351, October 2014.

[19] Arne Stormo, Olivier Lengliné, Jean Schmittbuhl, and Alex Hansen. Soft-clamp fiber bundle model and interfacial crack propagation: Comparison using a non-linear imposed displacement. *Frontiers in Physics*, 4, 2016.

[20] Jonas Tøgersen Kjellstadli. *Local versus Equal Load Sharing in the Fiber Bundle Model*. PhD thesis, NTNU, 2019.

[21] A. Garcimartín, A. Guarino, L. Bellon, and S. Ciliberto. Statistical Properties of Fracture Precursors. *Physical Review Letters*, 79(17):3202–3205, October 1997.

[22] L. I. Salminen, A. I. Tolvanen, and M. J. Alava. Acoustic emission from paper fracture. *Phys. Rev. Lett.*, 89:185503, Oct 2002.

[23] Per Bak, Chao Tang, and Kurt Wiesenfeld. Self-organized criticality: An explanation of the 1/f noise. *Phys. Rev. Lett.*, 59:381–384, Jul 1987.

[24] M. Kloster, Alex Hansen, and P. Hemmer. Burst avalanches in solvable models of fibrous materials. *Physical review. E, Statistical physics, plasmas, fluids, and related interdisciplinary topics*, 56, 03 1997.

[25] Santanu Sinha, Jonas T. Kjellstadli, and Alex Hansen. Local load-sharing fiber bundle model in higher dimensions. *Physical Review E*, 92(2):020401, August 2015.

[26] Stefano Zapperi, Purusattam Ray, H. Eugene Stanley, and Alessandro Vespignani. Avalanches in breakdown and fracture processes. *Physical Review E*, 59 (5):5049–5057, May 1999.

[27] Knut Jørgen Måløy, Stéphane Santucci, Jean Schmittbuhl, and Renaud Toussaint. Local Waiting Time Fluctuations along a Randomly Pinned Crack Front. *Physical Review Letters*, 96(4):045501, January 2006.

[28] Ken Tore Tallakstad, Renaud Toussaint, Stephane Santucci, Jean Schmittbuhl, and Knut Jørgen Måløy. Local dynamics of a randomly pinned crack front during creep and forced propagation: An experimental study. *Physical Review E*, 83(4):046108, April 2011.

[29] O. Lengliné, J.E. Elkhoury, G. Daniel, J. Schmittbuhl, R. Toussaint, J.-P. Ampuero, and M. Bouchon. Interplay of seismic and aseismic deformations during earthquake swarms: An experimental approach. *Earth and Planetary Science Letters*, 331-332:215–223, May 2012.

[30] V. I. Räisänen, M. J. Alava, and R. M. Nieminen. Fracture of three-dimensional fuse networks with quenched disorder. *Physical Review B*, 58(21):14288–14295, December 1998.

[31] Stefano Zapperi, Phani Kumar V. V. Nukala, and Srdan Šimunović. Crack roughness and avalanche precursors in the random fuse model. *Physical Review E*, 71(2):026106, February 2005.

[32] S. Lennartz-Sassinek, I. G. Main, M. Zaiser, and C. C. Graham. Acceleration and localization of subcritical crack growth in a natural composite material. *Physical Review E*, 90(5):052401, 2014.

[33] Attia Batool, Gergő Pál, Zsuzsa Danku, and Ferenc Kun. Transition from localized to mean field behaviour of cascading failures in the fiber bundle model on complex networks. *Chaos, Solitons and Fractals*, 159:112190, 2022.

[34] Sulochana Shrestha, Manigandan Kannan, Gregory N. Morscher, Michael J. Presby, and S. Mostafa Razavi. In-situ fatigue life analysis by modal acoustic emission, direct current potential drop and digital image correlation for steel. *International Journal of Fatigue*, 142:105924, 2021.

[35] Mengyu Chai, Jin Zhang, Zaoxiao Zhang, Quan Duan, and Guangxu Cheng. Acoustic emission studies for characterization of fatigue crack growth in 316LN stainless steel and welds. *Applied Acoustics*, 126:101–113, 2017.

[36] Jianguo Yu, Paul Ziehl, Boris Zárate, and Juan Caicedo. Prediction of fatigue crack growth in steel bridge components using acoustic emission. *Journal of Constructional Steel Research*, 67(8):1254–1260, August 2011.

[37] Jingmang Xu, Kai Wang, Qiantao Ma, Haoran Li, Ping Wang, Rong Chen, Yao Qian, and Dongfang Zeng. Study on acoustic emission properties and crack growth rate identification of rail steels under different fatigue loading conditions. *International Journal of Fatigue*, 172:107638, July 2023.

[38] P. Paris and F. Erdogan. A critical analysis of crack propagation laws. *Journal of Basic Engineering*, 85(4):528–533, 1963.

[39] D. Stauffer. Scaling theory of percolation clusters. *Physics Reports*, 54(1):1–73, 1979.

[40] Vincent Beffara. Hausdorff dimensions for SLE6. *The Annals of Probability*, 32 (3B), July 2004.

[41] Federico Camia and Charles M. Newman. Critical percolation exploration path and SLE6: a proof of convergence. *Probability Theory and Related Fields*, 139 (3-4):473–519, November 2007.

[42] Dietrich Stauffer and Ammon Aharony. *Introduction To Percolation Theory*. Taylor & Francis, 0 edition, December 2018.

[43] Jens Feder. *Fractals*. Springer US, Boston, MA, 1988.

[44] Jonas T. Kjellstadli, Eivind Bering, Martin Hendrick, Srutarshi Pradhan, and Alex Hansen. Can local stress enhancement induce stability in fracture processes? part i: Apparent stability. *Frontiers in Physics*, 7:105, 2019.

[45] Raul Cruz Hidalgo, Yamir Moreno, Ferenc Kun, and Hans J. Herrmann. Fracture model with variable range of interaction. *Physical Review E*, 65(4):046148, 2002.

[46] Soumyajyoti Biswas, Subhadeep Roy, and Purusattam Ray. Nucleation versus percolation: Scaling criterion for failure in disordered solids. *Physical Review E*, 91(5):050105, May 2015.